

Direct Diffusion Score Preference Optimization via Stepwise Contrastive Policy-Pair Supervision

Dohyun Kim¹ Seungwoo Lyu¹ Seung Wook Kim² Paul Hongsuck Seo¹

¹Dept. of CSE, Korea University ²NVIDIA

{a12s12, dbtmdnn41, phseo}@korea.ac.kr, seungwookk@nvidia.com

Abstract

Diffusion models have achieved impressive results in generative tasks such as text-to-image synthesis, yet they often struggle to fully align outputs with nuanced user intent and maintain consistent aesthetic quality. Existing preference-based training methods like Diffusion Direct Preference Optimization help address these issues but rely on costly and potentially noisy human-labeled datasets. In this work, we introduce Direct Diffusion Score Preference Optimization (DDSPO), which—when winning/losing policies are accessible—directly derives per-timestep supervision from these policies. Unlike prior methods that operate solely on final samples, DDSPO provides dense, transition-level signals across the denoising trajectory. In practice, we avoid reliance on labeled data by automatically generating preference signals using a pretrained reference model: we contrast its outputs when conditioned on original prompts versus semantically degraded variants. This practical strategy enables effective score-space preference supervision without explicit reward modeling or manual annotations. Empirical results demonstrate that DDSPO improves text-image alignment and visual quality, outperforming or matching existing preference-based methods while requiring significantly less supervision.

1. Introduction

Diffusion models [15, 45] have achieved impressive results across a variety of generative tasks, particularly in text-to-image synthesis [38, 42, 44, 46]. Despite this progress, they often struggle to fully align generated outputs with nuanced user intent and to consistently produce aesthetically high-quality images. Addressing these shortcomings typically requires task-specific training data, which can be difficult and costly to obtain. As an alternative, human preference annotations provide a lightweight yet expressive means of encoding such qualitative information in the form of ranked comparisons. Leveraging this, re-

cent approaches have incorporated human preferences into the training process, such as through reinforcement learning with human feedback (RLHF). A notable example is Diffusion DPO [52], which extends the Direct Preference Optimization (DPO) framework [41]—originally developed for language and vision-language models [41, 58, 59]—to diffusion models. Diffusion DPO enables models to learn directly from preference comparisons without requiring reward models. While effective, this approach relies heavily on labeled preference datasets, which are expensive to curate, limiting their scalability. In addition, Diffusion DPO receives supervision only from final samples, preventing the model from obtaining stepwise and dense learning signals along the denoising trajectory.

To overcome these limitations, we propose **Direct Diffusion Score Preference Optimization (DDSPO)**, a generalized variant of Diffusion DPO that formulates preference supervision in score space at each diffusion timestep rather than in the final sample space. Unlike prior approaches that define preferences over final samples $(\mathbf{x}_0^w, \mathbf{x}_0^l)$, DDSPO introduces stepwise supervision by comparing the denoising scores of a contrastive policy pair at each timestep. This is implemented by extending preference labels to tuples $((\mathbf{x}_t^w, \mathbf{x}_{t-1}^w), (\mathbf{x}_t^l, \mathbf{x}_{t-1}^l))$, derived from the contrastive policy pair, *i.e.*, preferred and dispreferred denoising policies. We define a score-space loss that optimizes the model’s denoising predictions toward targets ϵ_*^w and ϵ_*^l , corresponding to preferred and dispreferred behavior at each timestep. By deriving per-timestep targets from the contrastive policy pair, DDSPO enables richer supervision across denoising steps and reduces reliance on final outputs \mathbf{x}_0 . For practical use of DDSPO, we further introduce an instantiation of the contrastive policy pair using a pretrained reference model conditioned on original and perturbed prompts, which define the preferred and dispreferred denoising behaviors, respectively. Given an input prompt c and its semantically degraded variant c^- , we construct pseudo preference signals as follows: the reference model’s score prediction $\epsilon_{\text{ref}}(\mathbf{x}_t^w, t, c)$ is treated as the target for preferred denoising behavior, while $\epsilon_{\text{ref}}(\mathbf{x}_t^l, t, c^-)$ represents a dis-

preferred direction. The model is then trained to match the preferred score and to actively avoid the dispreferred score. This stepwise contrastive signal allows DDSPO to steer the model toward desirable generation behavior without any explicit preference annotations or reward modeling, making the method directly applicable even when human-labeled preference data is unavailable.

As a result, DDSPO consistently improves both text–image alignment and aesthetic quality—achieving performance competitive with or superior to existing preference-based approaches—demonstrating its practicality and broad applicability. Our main contributions are threefold:

- We propose DDSPO, a preference optimization framework that enables direct supervision over intermediate denoising steps in score space through a contrastive policy pair.
- We introduce a practical approach for constructing stepwise preference signals without any labeled datasets or reward models by leveraging prompt perturbation and a pretrained reference model.
- Extensive experiments show that DDSPO performs on par with or surpasses existing approaches that rely on external preference datasets or reward models, despite requiring neither.

2. Related work

Improving Diffusion Model Several lines of research [1, 7, 23, 25, 60, 61] have sought to improve diffusion models by incorporating external signals derived from human preferences. These approaches often rely on pretrained or learned reward models [1, 23, 25, 60], and formulate the generation process as a reinforcement learning (RL) problem [1, 7, 11, 61]. More recent work also explores combining multiple reward models or iteratively refining preferences [4, 12, 25, 39, 64, 66]. However, these methods still depend heavily on explicitly labeled preference data or pretrained reward models, incurring substantial annotation costs and computational overhead. In contrast, our work introduces a scalable alternative that requires neither reward models nor preference-labeled datasets, instead aligning diffusion models via contrastive signals obtained from prompt perturbations.

Direct Preference Optimization (DPO) Direct Preference Optimization (DPO) [41] has recently gained traction as a more direct and efficient way to align generative models with human preferences. Originally proposed for aligning large language models and vision-language models, DPO fine-tunes models using only paired preference data, bypassing the need for explicitly trained reward models [33, 59]. This leads to simpler training pipelines and improved alignment stability compared to reinforcement learning from human feedback. Diffusion DPO [52] ex-

tends DPO to diffusion models by re-formulating the objective to match the diffusion sampling process. Several subsequent works [5, 16, 28, 29, 65, 68] extend this paradigm in different ways, exploring alternative objectives and forms of preference supervision.

Self-Training Recent advances have shown that generative models can be effectively aligned with human preferences through self-training, without relying on paired preference data or externally trained reward models [3, 6, 8, 13, 19, 24, 37, 50, 54, 57, 63, 69, 70]. Especially for diffusion models, these methods typically involve generating synthetic preference signals from the model’s own outputs—contrasting higher-quality generations with intentionally degraded ones [37] or leveraging iterative refinements across model checkpoints [63]. By treating the model’s stronger outputs as preferred examples and weaker ones as negatives, they enable preference-aware fine-tuning through supervised objectives such as Direct Preference Optimization [37, 63]. In some cases, contrastive learning [24] or prompt relabeling [3] further reinforces semantic consistency and corrects misalignments. Our work follows this direction by using prompting techniques to automatically construct both positive and negative samples—not only final image pairs but also intermediate denoising score pairs—enabling the generalized DDSPO framework to operate without any human-labeled preference data.

3. Method

Our objective is to propose a novel optimization formulation for aligning pretrained diffusion models with desirable generation behavior, such as improved text-to-image alignment or aesthetic quality. We first review Direct Preference Optimization (DPO) [41] and its extension to diffusion models in Sec. 3.1, which assume access to preference-labeled final samples $(\mathbf{x}_0^w, \mathbf{x}_0^l \mid c)$. In Sec. 3.2, we introduce Direct Diffusion Score Preference Optimization (DDSPPO), which directly optimizes denoising behavior at each timestep using winning and losing denoising scores sampled from a contrastive policy pair as stepwise supervision. Sec. 3.3 describes a practical method for constructing such score-level preferences by leveraging a frozen pretrained reference model conditioned on perturbed prompts, eliminating the need for explicit labels. Finally, Sec. 3.4 compares DDSPO with existing diffusion preference-optimization methods, including Diffusion DPO [52], DSPO [68], and SPO [29], and discusses their conceptual and methodological differences in how preference signals are defined and utilized.

3.1. Preliminary

Direct Preference Optimization Direct Preference Optimization (DPO) [41] is a learning framework that aligns model outputs with human preferences by directly opti-

mizing on pairwise preference data. Given a conditioning input \mathbf{c} , we assume access only to preference-labeled pairs $(\mathbf{x}_0^w, \mathbf{x}_0^l \mid \mathbf{c})$, where \mathbf{x}_0^w denotes the preferred sample and \mathbf{x}_0^l the dispreferred one. The interpretation of \mathbf{c} and \mathbf{x}_0 depends on the task, where \mathbf{c} is a text caption and \mathbf{x}_0 is a synthesized image in text-to-image generation. Such preferences may reflect various notions of quality—such as semantic alignment, aesthetic appeal, or factual correctness—depending on the task context.

These preferences can be formalized using the Bradley–Terry model [2], which defines the following distribution:

$$\mathbb{P}(\mathbf{x}_0^w \succ \mathbf{x}_0^l \mid \mathbf{c}) = \sigma(r(\mathbf{c}, \mathbf{x}_0^w) - r(\mathbf{c}, \mathbf{x}_0^l)), \quad (1)$$

where $\mathbf{x}_0^w \succ \mathbf{x}_0^l$ denotes that \mathbf{x}_0^w is preferred over \mathbf{x}_0^l , $\sigma(\cdot)$ is the sigmoid function and $r(\mathbf{c}, \mathbf{x}_0)$ is a latent reward function that is difficult to access directly. DPO reparameterizes this setup to directly optimize the model distribution $p_\theta(\mathbf{x}_0 \mid \mathbf{c})$. It begins from the RLHF-style KL-regularized objective, which maximizes reward while constraining the learned distribution to stay close to a fixed reference distribution $p_{\text{ref}}(\mathbf{x}_0 \mid \mathbf{c})$:

$$\begin{aligned} \max_{\theta} \mathbb{E}_{\mathbf{x}_0 \sim p_\theta(\mathbf{x}_0 \mid \mathbf{c})} [r(\mathbf{c}, \mathbf{x}_0)] \\ - \beta \mathbb{D}_{\text{KL}}(p_\theta(\mathbf{x}_0 \mid \mathbf{c}) \parallel p_{\text{ref}}(\mathbf{x}_0 \mid \mathbf{c})) \end{aligned} \quad (2)$$

where β is a parameter that controls regularization strength. This objective admits a closed-form solution where the optimal distribution $p_\theta^*(\mathbf{x}_0 \mid \mathbf{c})$ is proportional to the reference distribution $p_{\text{ref}}(\mathbf{x}_0 \mid \mathbf{c})$ scaled by an exponential of the reward: $p_\theta^*(\mathbf{x}_0 \mid \mathbf{c}) \propto p_{\text{ref}}(\mathbf{x}_0 \mid \mathbf{c}) \cdot \exp(r(\mathbf{c}, \mathbf{x}_0) / \beta)$. This reformulation reveals that the reward function can be captured by the ratio between the optimized policy and the reference distribution, eliminating the need to model $r(\mathbf{c}, \mathbf{x}_0)$ explicitly. This leads to the DPO training objective:

$$\begin{aligned} \mathcal{L}_{\text{DPO}}(\theta) = -\mathbb{E}_{\mathbf{c}, \mathbf{x}_0^w, \mathbf{x}_0^l} \log \sigma \left(\right. \\ \left. \beta \log \frac{p_\theta(\mathbf{x}_0^w \mid \mathbf{c})}{p_{\text{ref}}(\mathbf{x}_0^w \mid \mathbf{c})} - \beta \log \frac{p_\theta(\mathbf{x}_0^l \mid \mathbf{c})}{p_{\text{ref}}(\mathbf{x}_0^l \mid \mathbf{c})} \right). \end{aligned} \quad (3)$$

DPO for Diffusion Models Applying DPO to diffusion models introduces a unique challenge: directly computing the log-likelihood ratio $\log \frac{p_\theta(\mathbf{x}_0 \mid \mathbf{c})}{p_{\text{ref}}(\mathbf{x}_0 \mid \mathbf{c})}$ is intractable due to the need to marginalize over all possible diffusion trajectories $x_{1:T}$ that generate \mathbf{x}_0 . To circumvent this, [52] reformulates the objective over entire denoising paths and approximate the reverse process $p_\theta(x_{1:T} \mid \mathbf{x}_0)$ using the forward noising process $q(x_{1:T} \mid \mathbf{x}_0)$. This reparameterization enables training in the *score space*, where models learn to predict the noise (or equivalently, the score function [15, 51]) that

guides the denoising process:

$$\begin{aligned} \mathcal{L}(\theta) = -\mathbb{E}_{\substack{(\mathbf{x}_0^w, \mathbf{x}_0^l) \sim \mathcal{D}, t \sim \mathcal{U}(0, T), \\ \mathbf{x}_t^w \sim q(\mathbf{x}_t^w \mid \mathbf{x}_0^w), \mathbf{x}_t^l \sim q(\mathbf{x}_t^l \mid \mathbf{x}_0^l)}} \log \sigma \left(-\beta \cdot [\right. \\ \left. \|\boldsymbol{\epsilon}^w - \boldsymbol{\epsilon}_\theta(\mathbf{x}_t^w, t, \mathbf{c})\|_2^2 - \|\boldsymbol{\epsilon}^w - \boldsymbol{\epsilon}_{\text{ref}}(\mathbf{x}_t^w, t, \mathbf{c})\|_2^2 \right. \\ \left. - (\|\boldsymbol{\epsilon}^l - \boldsymbol{\epsilon}_\theta(\mathbf{x}_t^l, t, \mathbf{c})\|_2^2 - \|\boldsymbol{\epsilon}^l - \boldsymbol{\epsilon}_{\text{ref}}(\mathbf{x}_t^l, t, \mathbf{c})\|_2^2)] \right) \end{aligned}$$

where $\mathbf{x}_t^* = \alpha_t \mathbf{x}_0^* + \sigma_t \boldsymbol{\epsilon}^*$ is drawn from $q(\mathbf{x}_t^* \mid \mathbf{x}_0^*)$, and $\boldsymbol{\epsilon}^* \sim \mathcal{N}(0, I)$. The term $\|\boldsymbol{\epsilon}^w - \boldsymbol{\epsilon}_\theta(\mathbf{x}_t^w, t, \mathbf{c})\|_2^2 - \|\boldsymbol{\epsilon}^w - \boldsymbol{\epsilon}_{\text{ref}}(\mathbf{x}_t^w, t, \mathbf{c})\|_2^2$ penalizes the student whenever its predicted score at \mathbf{x}_t^w is farther from the target $\boldsymbol{\epsilon}^w$ than the reference model, thereby pushing it closer to $\boldsymbol{\epsilon}^w$. The analogous term for \mathbf{x}_t^l pushes the student away from $\boldsymbol{\epsilon}^l$ relative to the reference, producing a pairwise preference signal. However, both $\boldsymbol{\epsilon}^w$ and $\boldsymbol{\epsilon}^l$ originate from samples $\mathbf{x}_t^* \sim q(\mathbf{x}_t^* \mid \mathbf{x}_0^*)$, so supervision at timestep t ultimately stems only from the final samples $(\mathbf{x}_0^w, \mathbf{x}_0^l)$ rather than providing supervision over the intermediate denoising steps. Full derivations of both the standard and diffusion DPO objectives are provided in the Supp. Mat.

3.2. Direct Diffusion Score Preference Optimization

We now consider a setting in which preference is defined not over final generated samples, but over a transition between intermediate denoising steps. Crucially, rather than assuming access only to preference-labeled final samples $(\mathbf{x}_0^w, \mathbf{x}_0^l \mid \mathbf{c})$, we also assume access to preference-labeled denoising transitions at intermediate steps. Let $p_\star^w(\mathbf{x}_{t-1, t} \mid \mathbf{c})$ and $p_\star^l(\mathbf{x}_{t-1, t} \mid \mathbf{c})$ denote the winning and losing denoising policies, forming a contrastive policy pair. Sampling from these policies yields tuples $((\mathbf{x}_t^w, \mathbf{x}_{t-1}^w), (\mathbf{x}_t^l, \mathbf{x}_{t-1}^l) \mid \mathbf{c})$. This enables direct preference of denoising behavior at each timestep of the diffusion process.

Following the Bradley–Terry formulation in Eq. (1), we extend the preference supervision from final outputs $(\mathbf{x}_0^w, \mathbf{x}_0^l \mid \mathbf{c})$ to denoising transitions at intermediate steps, using tuples of the form $((\mathbf{x}_t^w, \mathbf{x}_{t-1}^w), (\mathbf{x}_t^l, \mathbf{x}_{t-1}^l) \mid \mathbf{c})$. The reward function is accordingly redefined as $r(\mathbf{c}, \mathbf{x}_t, \mathbf{x}_{t-1})$, and preferences are modeled over entire denoising transitions. By applying the same derivation steps as in Eqs. (1) to (3), and extending the supervision to denoising transitions at arbitrary diffusion timesteps $t \sim \mathcal{U}(0, T)$ the loss can be analogously formulated as:

$$\begin{aligned} \mathcal{L}(\theta) = -\mathbb{E}_{\mathbf{c} \sim \mathcal{D}(\mathbf{c}), t \sim \mathcal{U}(0, T), (\mathbf{x}_{t-1}^w, \mathbf{x}_t^w), (\mathbf{x}_{t-1}^l, \mathbf{x}_t^l)} \\ \log \sigma \left(\beta \log \frac{p_\theta(\mathbf{x}_{t-1}^w \mid \mathbf{x}_t^w, \mathbf{c})}{p_{\text{ref}}(\mathbf{x}_{t-1}^w \mid \mathbf{x}_t^w, \mathbf{c})} - \beta \log \frac{p_\theta(\mathbf{x}_{t-1}^l \mid \mathbf{x}_t^l, \mathbf{c})}{p_{\text{ref}}(\mathbf{x}_{t-1}^l \mid \mathbf{x}_t^l, \mathbf{c})} \right), \end{aligned}$$

where $(\mathbf{x}_{t-1}^w, \mathbf{x}_t^w) \sim p_\star^w(\mathbf{x}_{t-1, t}^w \mid \mathbf{c})$, $(\mathbf{x}_{t-1}^l, \mathbf{x}_t^l) \sim p_\star^l(\mathbf{x}_{t-1, t}^l \mid \mathbf{c})$. Since the joint transition distribution $p_\star^w(\mathbf{x}_{t-1, t}^w \mid \mathbf{c})$ is generally intractable, we approximate it

as $p_{\star}^w(\mathbf{x}_{t-1,t}^w \mid \mathbf{c}) \approx q(\mathbf{x}_t^w \mid \mathbf{x}_0^w) p_{\star}^w(\mathbf{x}_{t-1}^w \mid \mathbf{x}_t^w, \mathbf{c})$, where $\mathbf{x}_0^w \sim \mathcal{D}$, $\mathbf{x}_t^w \sim q(\mathbf{x}_t^w \mid \mathbf{x}_0^w)$, and $\mathbf{x}_{t-1}^w \sim p_{\star}^w(\mathbf{x}_{t-1}^w \mid \mathbf{x}_t^w, \mathbf{c})$. This provides a practical sampling scheme in which the preferred transition is constructed by forward noising followed by preference-guided denoising. An analogous approximation is applied to the dispreferred transition $p_{\star}^l(\mathbf{x}_{t-1}^l \mid \mathbf{x}_t^l, \mathbf{c})$. Under this approximation, we derive the following score-space objective [51]; see Supp. Mat. for the full derivation:

$$\begin{aligned} \mathcal{L}_{\text{DDSPo}}(\theta) &= -\mathbb{E}_{(\mathbf{x}_0^w, \mathbf{x}_0^l) \sim \mathcal{D}, \mathbf{c} \sim \mathcal{D}(\mathbf{c}), t \sim \mathcal{U}(0, T),} \\ &\quad \mathbf{x}_t^w \sim q(\mathbf{x}_t^w \mid \mathbf{x}_0^w), \mathbf{x}_t^l \sim q(\mathbf{x}_t^l \mid \mathbf{x}_0^l) \\ &\log \sigma \left(-\beta \cdot [\|\boldsymbol{\epsilon}_{\star}^w - \boldsymbol{\epsilon}_{\theta}(\mathbf{x}_t^w, t, \mathbf{c})\|_2^2 - \|\boldsymbol{\epsilon}_{\star}^w - \boldsymbol{\epsilon}_{\text{ref}}(\mathbf{x}_t^w, t, \mathbf{c})\|_2^2 \right. \\ &\quad \left. - (\|\boldsymbol{\epsilon}_{\star}^l - \boldsymbol{\epsilon}_{\theta}(\mathbf{x}_t^l, t, \mathbf{c})\|_2^2 - \|\boldsymbol{\epsilon}_{\star}^l - \boldsymbol{\epsilon}_{\text{ref}}(\mathbf{x}_t^l, t, \mathbf{c})\|_2^2)] \right). \quad (4) \end{aligned}$$

Here, $\boldsymbol{\epsilon}_{\star}^w$, $\boldsymbol{\epsilon}_{\star}^l$ denote denoising score targets obtained from the contrastive policy pair— $p_{\star}^w(\mathbf{x}_{t-1}^w \mid \mathbf{x}_t^w, \mathbf{c})$ and $p_{\star}^l(\mathbf{x}_{t-1}^l \mid \mathbf{x}_t^l, \mathbf{c})$ —thereby enabling direct preference optimization in diffusion score space at each timestep.

3.3. DDSPo in Practical Use

contrastive policy pair In practice, direct supervision over intermediate transition preferences, in the form of denoising score pairs $(\boldsymbol{\epsilon}_{\star}^w, \boldsymbol{\epsilon}_{\star}^l)$, is rarely available. To address this, we introduce a practical and effective strategy for generating such signals based on prompt perturbation. Specifically, we treat the denoising score predicted from the original prompt \mathbf{c} as the preferred signal, and construct a dispreferred counterpart by generating a corrupted version of the prompt \mathbf{c}^- and computing the corresponding denoising score. Note that the type of perturbation applied to the prompt may vary depending on the specific application of preference optimization (e.g., text-to-image alignment or aesthetic quality). These signals can be obtained using a pretrained reference model. In this setup, the noise $\boldsymbol{\epsilon}_{\text{ref}}(\mathbf{x}_t^w, t, \mathbf{c})$ guided by \mathbf{c} is considered positively aligned with the intended semantics, while the noise $\boldsymbol{\epsilon}_{\text{ref}}(\mathbf{x}_t^l, t, \mathbf{c}^-)$ from \mathbf{c}^- is dispreferred, as it reflects guidance from an incomplete or misleading prompt. By plugging these noises as supervision targets into the DDSPo objective in Eq. (4), we get

$$\begin{aligned} \mathcal{L}(\theta) &= -\mathbb{E}_{(\mathbf{x}_0^w, \mathbf{x}_0^l) \sim \mathcal{D}, (\mathbf{c}, \mathbf{c}^-) \sim \mathcal{D}(\mathbf{c}), t \sim \mathcal{U}(0, T),} \\ &\quad \mathbf{x}_t^w \sim q(\mathbf{x}_t^w \mid \mathbf{x}_0^w), \mathbf{x}_t^l \sim q(\mathbf{x}_t^l \mid \mathbf{x}_0^l) \\ &\quad \log \sigma \left(-\beta \cdot [\right. \\ &\quad \left. \|\boldsymbol{\epsilon}_{\text{ref}}(\mathbf{x}_t^w, t, \mathbf{c}) - \boldsymbol{\epsilon}_{\theta}(\mathbf{x}_t^w, t, \mathbf{c})\|_2^2 \right. \\ &\quad \left. - \|\boldsymbol{\epsilon}_{\text{ref}}(\mathbf{x}_t^w, t, \mathbf{c}) - \boldsymbol{\epsilon}_{\text{ref}}(\mathbf{x}_t^w, t, \mathbf{c})\|_2^2 \right. \\ &\quad \left. - (\|\boldsymbol{\epsilon}_{\text{ref}}(\mathbf{x}_t^l, t, \mathbf{c}^-) - \boldsymbol{\epsilon}_{\theta}(\mathbf{x}_t^l, t, \mathbf{c})\|_2^2 \right. \\ &\quad \left. - \|\boldsymbol{\epsilon}_{\text{ref}}(\mathbf{x}_t^l, t, \mathbf{c}^-) - \boldsymbol{\epsilon}_{\text{ref}}(\mathbf{x}_t^l, t, \mathbf{c})\|_2^2)] \right) \quad (5) \end{aligned}$$

Here, the term $\|\boldsymbol{\epsilon}_{\text{ref}}(\mathbf{x}_t^w, t, \mathbf{c}) - \boldsymbol{\epsilon}_{\theta}(\mathbf{x}_t^w, t, \mathbf{c})\|_2^2 - \|\boldsymbol{\epsilon}_{\text{ref}}(\mathbf{x}_t^w, t, \mathbf{c}) - \boldsymbol{\epsilon}_{\text{ref}}(\mathbf{x}_t^w, t, \mathbf{c})\|_2^2$ simplifies to a stan-

dard distillation loss, as the second term vanishes. This encourages the student model to closely follow the reference without degrading its original capabilities. In contrast, the term $\|\boldsymbol{\epsilon}_{\text{ref}}(\mathbf{x}_t^l, t, \mathbf{c}^-) - \boldsymbol{\epsilon}_{\theta}(\mathbf{x}_t^l, t, \mathbf{c})\|_2^2 - \|\boldsymbol{\epsilon}_{\text{ref}}(\mathbf{x}_t^l, t, \mathbf{c}^-) - \boldsymbol{\epsilon}_{\text{ref}}(\mathbf{x}_t^l, t, \mathbf{c})\|_2^2$ penalizes the model when its prediction moves closer to the degraded direction $\boldsymbol{\epsilon}_{\text{ref}}(\mathbf{x}_t^l, t, \mathbf{c}^-)$ than the reference model’s own output does. Together, these two terms encourage the model to retain useful denoising capabilities while avoiding alignment with poor or corrupted guidance signals. Note that while prompt perturbation has been used in other domains to construct synthetic preference data, DDSPo is the first to extend this idea to step-wise score pairs, enabling supervision at every denoising step.

Training Pipeline We focus on a setup without preference-labeled image pairs, as domain-specific preference datasets are often unavailable in practice. Thus, we construct an image preference dataset $\mathcal{D} = \{(\mathbf{x}_0^w, \mathbf{x}_0^l, \mathbf{c}, \mathbf{c}^-)\}$ by generating $(\mathbf{x}_0^w, \mathbf{x}_0^l)$ from the reference model for each prompt pair $(\mathbf{c}, \mathbf{c}^-)$. During training, we sample $(\mathbf{x}_0^w, \mathbf{x}_0^l, \mathbf{c}, \mathbf{c}^-) \sim \mathcal{D}$, draw $t \sim \mathcal{U}\{1, \dots, T\}$, obtain $\mathbf{x}_t^w \sim q(\mathbf{x}_t^w \mid \mathbf{x}_0^w)$ and $\mathbf{x}_t^l \sim q(\mathbf{x}_t^l \mid \mathbf{x}_0^l)$ via the forward process. We then compute the denoising score targets $\boldsymbol{\epsilon}_{\text{ref}}(\mathbf{x}_t^w, t, \mathbf{c})$ and $\boldsymbol{\epsilon}_{\text{ref}}(\mathbf{x}_t^l, t, \mathbf{c}^-)$ from the frozen reference model, and optimize Eq. (5).

Efficient DDSPo without Image Preference Pair Dataset Motivated by recent findings [21] that effective score distillation does not require strict pairing between the noised image \mathbf{x}_t and the conditioning prompt \mathbf{c} (e.g., at large t the distribution of \mathbf{x}_t is approximately standard Gaussian regardless of \mathbf{x}_0 , and reverse generation is driven by the conditioning prompt, so strict prompt–image pairing is unnecessary to obtain meaningful signals), we introduce an efficient variant of DDSPo that avoids explicitly collecting dispreferred images. In practical settings where no ground-truth dispreferred images exist, a naïve approach would be to generate a dispreferred sample \mathbf{x}_0^l for every perturbed prompt $(\mathbf{c}, \mathbf{c}^-)$, but this is computationally expensive. Instead, we can reuse a randomly sampled positive image \mathbf{x}_0^+ (from another prompt) as a surrogate for \mathbf{x}_0^l , obtain $\mathbf{x}_t^l \sim q(\mathbf{x}_t^l \mid \mathbf{x}_0^+)$ via the forward process, and estimate the losing direction using the perturbed prompt \mathbf{c}^- (e.g., compute $\boldsymbol{\epsilon}_{\text{ref}}(\mathbf{x}_t^l, t, \mathbf{c}^-)$). Although this introduces a prompt–image mismatch on the losing branch, the conditioning still provides a meaningful negative direction—especially at larger timesteps—and aggregation across timesteps and prompts yields informative supervision. In practice, this design cuts the cost of collecting additional dispreferred samples, showing the flexibility of DDSPo in positive-only settings.

3.4. Relationship to Previous Work

Diffusion DPO as a Special Case of DDSPo While DDSPo uses $p_{\star}^*(\mathbf{x}_{t-1}^* \mid \mathbf{x}_t^*, \mathbf{c})$ as the contrastive policy pair, Diffusion DPO is a special case of DDSPo that de-

fines $p_{\star}^*(\mathbf{x}_{t-1}^* \mid \mathbf{x}_t^*, \mathbf{c}) \triangleq q(\mathbf{x}_{t-1}^* \mid \mathbf{x}_t^*, \mathbf{x}_0^*)$. This shifts the notion of preference toward the final outputs, making the model heavily reliant on \mathbf{x}_0^w and \mathbf{x}_0^l . Consequently, supervision is broadcast from these final samples to all timesteps and, especially at large t , can be broad and unspecific. In contrast, DDSPO supervises each local transition $\mathbf{x}_t \rightarrow \mathbf{x}_{t-1}$ under the winning or losing denoising policies $p_{\star}(\mathbf{x}_{t-1} \mid \mathbf{x}_t, \mathbf{c})$, yielding more informative, dense, and localized timestep-specific signals and reducing sensitivity to noise in the final samples.

Relationship to DSPO DSPO [68] reinterprets preference alignment through a score-matching formulation by constructing a preference-adjusted target score—formed by combining the data score with a preference-derived score term—and fine-tuning the pretrained diffusion model to match this target. Concretely, DSPO defines a score-matching style objective of the form

$$\begin{aligned} \mathcal{L}_{\text{DSPO}}(\theta) = & \mathbb{E}_{(\mathbf{x}_0^w, \mathbf{x}_0^l), \mathbf{c}, t} A(t) \left\| (\epsilon_{\theta}(\mathbf{x}_t^w, t, \mathbf{c}) - \epsilon^w) \right. \\ & - \beta \left(1 - \sigma(r_{\theta}(\mathbf{x}_t^w, t, \mathbf{c}) - r_{\theta}(\mathbf{x}_t^l, t, \mathbf{c})) \right) \\ & \cdot \left. (\epsilon_{\theta}(\mathbf{x}_t^w, t, \mathbf{c}) - \epsilon_{\text{ref}}(\mathbf{x}_t^w, t, \mathbf{c})) \right\|_2^2. \quad (6) \end{aligned}$$

where $(\mathbf{x}_0^w, \mathbf{x}_0^l) \sim \mathcal{D}$, $\mathbf{c} \sim \mathcal{D}(\mathbf{c})$, $t \sim \mathcal{U}(0, T)$, $\mathbf{x}_t^w \sim q(\mathbf{x}_t^w \mid \mathbf{x}_0^w)$, $\mathbf{x}_t^l \sim q(\mathbf{x}_t^l \mid \mathbf{x}_0^l)$. Here, $A(t)$ is a timestep-dependent weighting function determined by the diffusion noise schedule, and $r_{\theta}(\mathbf{x}_t, t, \mathbf{c})$ is defined as

$$r_{\theta}(\mathbf{x}_t, t, \mathbf{c}) = \|\epsilon - \epsilon_{\theta}(\mathbf{x}_t, t, \mathbf{c})\|_2^2 - \|\epsilon - \epsilon_{\text{ref}}(\mathbf{x}_t, t, \mathbf{c})\|_2^2,$$

where denoising score target $\epsilon \sim \mathcal{N}(0, I)$ is derived by approximating $p_{\theta}(\mathbf{x}_{t-1} \mid \mathbf{x}_t, \mathbf{c})$ with the forward process $q(\mathbf{x}_{t-1} \mid \mathbf{x}_t, \mathbf{x}_0)$, so that the preference signal at timestep t is still induced from preference-labeled final samples via a forward-process approximation.

In contrast, DDSPO removes reliance on the forward process by deriving preference supervision directly from the contrastive denoising policies— $p_{\star}^w(\mathbf{x}_{t-1}^w \mid \mathbf{x}_t^w, \mathbf{c})$ and $p_{\star}^l(\mathbf{x}_{t-1}^l \mid \mathbf{x}_t^l, \mathbf{c}^-)$ —which provide per-step, policy-grounded preference signals. We can incorporate our per-step preference supervision into the DSPO by redefining

$$r_{\theta}(\mathbf{x}_t, t, \mathbf{c}) = \|\epsilon_{\star} - \epsilon_{\theta}(\mathbf{x}_t, t, \mathbf{c})\|_2^2 - \|\epsilon_{\star} - \epsilon_{\text{ref}}(\mathbf{x}_t, t, \mathbf{c})\|_2^2,$$

where ϵ_{\star}^w and ϵ_{\star}^l denote denoising score targets derived from the contrastive policy pair—the winning and losing denoising policies $p_{\star}^w(\mathbf{x}_{t-1}^w \mid \mathbf{x}_t^w, \mathbf{c})$ and $p_{\star}^l(\mathbf{x}_{t-1}^l \mid \mathbf{x}_t^l, \mathbf{c})$, respectively, as defined in DDSPO. In practice, these targets can be obtained from the reference model as $\epsilon_{\text{ref}}(\mathbf{x}_t^w, t, \mathbf{c})$ and $\epsilon_{\text{ref}}(\mathbf{x}_t^l, t, \mathbf{c}^-)$. This reformulation extends DSPO to operate in a stepwise manner, providing dense, per-step supervision analogous to DDSPO, with the detailed derivation and empirical results are provided in Supp. Mat. and Sec. 4.2, respectively.

Relationship to SPO Similar to DDSPO, Step-by-step Preference Optimization (SPO) [29] also introduces stepwise supervision along the denoising trajectory. At each timestep, SPO samples multiple candidates from a shared noisy latent \mathbf{x}_t and selects a win–lose pair $(\mathbf{x}_{t-1}^w, \mathbf{x}_{t-1}^l)$ based on a step-aware reward model pretrained to assess visual quality. Unlike prior DPO methods that propagate preference labels from final sample pairs across entire trajectories, SPO determines preference locally within a single denoising step using this pretrained reward model, enabling the model to identify preferences focusing on subtle, fine-grained visual details—such as texture, lighting, or color tone—rather than high-level semantic or layout features. This design effectively enhances image aesthetics by emphasizing nuanced human aesthetic preferences driven by these subtle visual cues; however, as reported in the original paper [29], SPO offers limited improvement for text–image alignment and cannot be directly applied to deterministic flow-matching models [31, 56] due to its reliance on stochastic candidate sampling. In contrast, DDSPO achieves stepwise supervision without such restrictions by directly deriving preference signals from contrastive policy pairs generated via prompt perturbations. This formulation is effective for both aesthetic enhancement and text-to-image alignment, and can be applied to both diffusion and flow-based generative models. Moreover, unlike SPO, DDSPO requires no auxiliary reward model or labeled preference data, as prompt perturbations intrinsically yield dense, stepwise training signals that enable free and scalable preference alignment. We empirically validate these properties across diverse architectures and tasks in Sec. 4.

4. Experiments

We assess the effectiveness of DDSPO on a range of conditional generation tasks, focusing on its ability to improve alignment and perceptual quality. We focus on scenarios where human-labeled preference data are not readily available—a common situation across many practical domains—and therefore generate preference data via perturbed prompting. Note that the preference datasets used in prior studies [23, 64] are currently not publicly accessible. In this section, we begin with a controlled 2D toy experiment (Sec. 4.1) to validate DDSPO’s core mechanism under minimal conditions. We then apply DDSPO to two practical text-to-image tasks: improving prompt-image alignment (Sec. 4.2) and enhancing aesthetic quality (Sec. 4.3). Finally, we explore the different prompt perturbation methods together with its efficient variant (Sec. 4.4).

4.1. Preliminary Experiments

We first conduct toy experiments to evaluate the effectiveness of DDSPO in a controlled 2D setting. Specifically, we simulate a simplified conditional generation task where

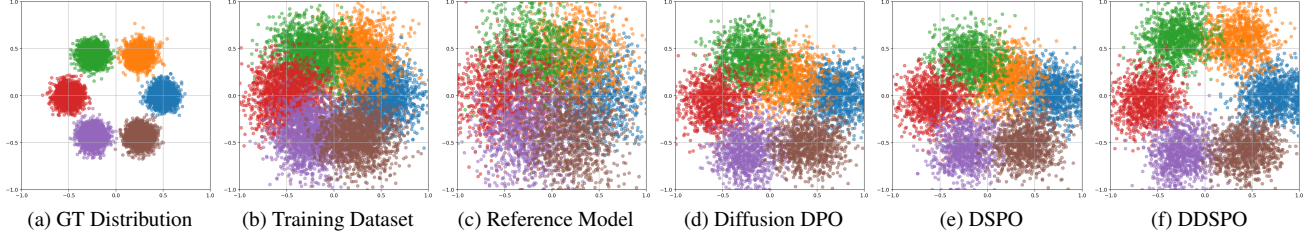


Figure 1. **Toy Experiments Comparison of Diffusion DPO (D-DPO), DSPO and DDSPO.** (a) and (b) show samples from the ground-truth distribution and its noisy variant used for training. (c) is generated by the reference diffusion model trained on (b). (d), (e) and (f) are distributions learned by the models finetuned with Diffusion DPO, DSPO and DDSPO, respectively.

each condition corresponds to a distinct mode of a multi-modal Gaussian distribution, as illustrated in Fig. 1a. A reference model is trained on a noisy dataset shown in Fig. 1b, mimicking real-world scenarios with imperfect supervision. The learned distribution from this reference model, shown in Fig. 1c, closely resembles the noisy training distribution. To construct preference data, we sample $N = 2$ preference pairs per class, each consisting of a preferred sample \mathbf{x}_0^w from the target class c and a dispreferred sample \mathbf{x}_0^l from a neighboring class c^- , simulating our perturbed prompting strategy. This dataset is then used to finetune the model using Diffusion DPO (D-DPO) [52], DSPO [68], and DDSPO. Among them, D-DPO and DSPO serve as baselines that obtain supervision only from preference-labeled final samples, whereas DDSPO leverages intermediate score preferences at each timestep t .

As shown in Figs. 1d and 1e, the baseline models finetuned with D-DPO and DSPO often fail to maintain clear separation between modes, resulting in overlapping or distorted output distributions. This issue becomes more pronounced when the fine-tuning dataset is smaller (see Supp. Mat. for extended results). The degradation arises because these baselines rely on denoising targets derived from potentially misaligned final samples, which can provide misleading learning signals as D-DPO always provides noise towards this particular final sample, as discussed in Sec. 3.2. In contrast, DDSPO enables the model to learn well-separated, condition-specific outputs, as shown in Fig. 1f. Rather than relying on a final samples (which can induce global, coarse signals), DDSPO directly models preference at each t by contrasting the winning and losing denoising policies p_*^w and p_*^l over the local transition $(\mathbf{x}_t \rightarrow \mathbf{x}_{t-1})$. This leads to more robust learning signals across the trajectory of denoising. Note that in the Fig. 1f, slight shifts of the centers away from zero can occur because DDSPO separates distributions across conditions by following the “winning” direction while pushing away from the “losing” (neighboring) direction in score space, yielding clearer boundaries between adjacent conditional distributions. In more complex, real-world tasks such as image generation, the condition space (*e.g.*, text space) is far more

Table 1. **Comparison of Preference Optimization Methods.** We evaluate D-DPO, DSPO, DSPO+CPP (our stepwise reformulation of DSPO with contrastive policy pair (CPP) described in Sec. 3.4), and DDSPO across GenEval, T2I-CompBench, FID, and IS, using identical perturbation-based preference data.

Model	GE \uparrow	CB \uparrow	FID \downarrow	IS \uparrow
SD-1.4	.4245	.3150	13.05	36.76
+D-DPO	.4841	.3723	18.02	36.64
+DSPO	.4841	.3793	18.28	35.87
+DSPO+CPP (Ours)	.4978	.3854	17.12	37.47
+DDSPO (Ours)	.5045	.3823	16.39	38.10

densely packed, providing supervision that contrasts across a wider range of diverse directions.

4.2. Improving Text-to-Image Alignment

Target Task We evaluate DDSPO for improving text-to-image alignment in diffusion models, enabling more faithful generation with respect to the input prompt.

Experimental Setup We evaluate DDSPO on text-to-image alignment tasks using pretrained diffusion models. A preference dataset is constructed by sampling 200K prompts from DiffusionDB [53], which serve as the original conditions c . For each prompt c , we generate a perturbed caption c^- by randomly removing 40% to 70% of the tokens, thereby reducing semantic specificity and content richness. To assess text-to-image alignment, we evaluate each model on the GenEval [9] and T2I-CompBench [18] benchmarks, which are designed to measure compositional and semantic consistency between text prompts and generated images. Additionally, we compute the Fréchet Inception Distance (FID) [14] and Inception Score (IS) [47] on 30K images generated from MS-COCO [30] validation prompts to assess output quality and diversity.

Comparisons of Preference Optimization Methods We finetune Stable Diffusion v1.4 (SD-1.4) [43] using D-DPO [52], DSPO [68], DSPO+CPP (our stepwise reformulation of DSPO with contrastive policy pair (CPP) described in Sec. 3.4), and DDSPO, and compare their performance in Tab. 1. While all methods exhibit performance gains, the proposed DDSPO achieves the most sub-

Table 2. **DDSPO on diverse backbones.** We evaluate DDSPO across Diverse Backbones (SD-1.4 [43], SDXL [38], SANA [56]).

Model	GenEval \uparrow	T2I-Compbench \uparrow
SD-1.4	.4245	.3150
+DDSPO	.5045	.3723
SDXL	.5229	.4034
+DDSPO	.6049	.4857
SANA	.6812	.4846
+DDSPO	.7266	.5255

Table 3. **Text-to-Image Alignment Comparisons to SOTA Methods.** Following CaPO’s evaluation protocol, we assess SDXL alongside its Itercomp, CaPO, and DDSPO variants.

Model	External Dependency	GenEval \uparrow	T2I-Compbench \uparrow
SDXL	-	.5229	.4185
+Itercomp	✓	.6108	.4644
+CaPO	✓	.5900	.4652
+DDSPO	✗	.6049	.5064

stantial improvements in alignment metrics (GenEval and T2I-CompBench). Furthermore, it attains higher IS, as the strengthened alignment encourages the model to generate more distinct and well-separated representations in the feature space. We also observe that fine-tuning with preference optimization generally introduces domain shifts from the MS-COCO image distribution; however, DDSPO remains closer to the original distribution while achieving the largest alignment improvements. Finally, incorporating our score-based preferences into DSPO also enhances performance, highlighting the advantage of score-level supervision even for preference optimization in the score-matching framework.

DDSPO with Various Model Architectures We apply DDSPO to models with three different architectures, including both U-Net-based models (SD-1.4 [43] and SDXL [38]) and a DiT-based flow-matching model (SANA [56]), as shown in Tab. 2. The results clearly demonstrate that DDSPO significantly improves text-to-image alignment across all three models on both benchmarks, highlighting its effectiveness and broad applicability across diverse diffusion architectures.

Comparisons to SOTA Methods In Tab. 3, we compare our method against current SOTA approaches, Itercomp [64] and CaPO [26], for improving text-to-image alignment. Notably, IterComp and CaPO rely on human-annotated datasets or reward models for training. In contrast, DDSPO achieves comparable performance on GenEval and outperforms all methods on CompBench, despite not using any human annotations, demonstrating its effectiveness in a data efficient setup. Qualitative results comparing the baseline SDXL model and the DDSPO-finetuned model can be found in Fig. 2.

Table 4. **Aesthetic Quality Comparison with SOTA Methods.** We compare our DDSPO with existing methods that rely on human-labeled supervision from Pick-a-Pic, whereas DDSPO is trained without human-labeled data.

Model	Dataset	HPSv2 \uparrow	PickScore \uparrow
SD-1.5	-	26.95	21.14
+D-DPO	Pickapic	27.25	21.34
+D-KTO	Pickapic	27.89	21.39
+SPO	Pickapic	27.50	21.41
+DDSPO	None	27.46	21.35
SDXL	-	27.89	22.27
+D-DPO	Pickapic	28.55	22.61
+MAPO	Pickapic	28.22	22.30
+SPO	Pickapic	29.21	23.11
+DDSPO	None	28.78	22.70

4.3. Improving Aesthetic Quality

Target Task In this section, we apply DDSPO to improve the aesthetic quality of images generated by diffusion models, promoting visually appealing and artistically coherent outputs.

Experimental Setup We evaluate the effectiveness of DDSPO in enhancing aesthetic quality with SD-1.5 [44] and SDXL [38]. Following the same training setup as in Sec. 4.2, we construct supervision pairs using sampled prompt pairs (c, c^-) , where the negative prompts c^- are generated by prompting LLaMA3-8B [10] to intentionally degrade the aesthetic quality of the original prompt. The prompt template used for generation is provided in the Supp. Mat. To evaluate aesthetic quality, we use the HPSv2 [55] and PickScore [23] metrics, both of which are measured by a model trained to reflect human aesthetic preferences using Human Preference Dataset v2 [55] and Pick-a-Pic [23], respectively. For evaluation, we generate images by sampling from prompts in the HPSv2 [55] and PartiPrompts [62] benchmarks, and assess them using the corresponding metrics.

Results In Tab. 4, we compare DDSPO with SOTA methods for aesthetic quality improvement, including D-DPO [52], Diffusion KTO (D-KTO) [28], SPO [29] and MAPO [16]. DDSPO significantly improves both HPSv2 and PickScore compared to the two baselines (SD-1.5 and SDXL). Notably, DDSPO is trained solely on automatically constructed preference data using perturbed prompts, while all competing methods rely on human-annotated preference labels. Despite this, DDSPO achieves comparable performance across all evaluation metrics, highlighting its effectiveness in the absence of human supervision.

4.4. Preference Score Pairs by Perturbed Prompts

Effects of Different Perturbed Prompts Tab. 5 presents an exploration of different prompt perturbation strategies for constructing dispreferred scores across the two previ-

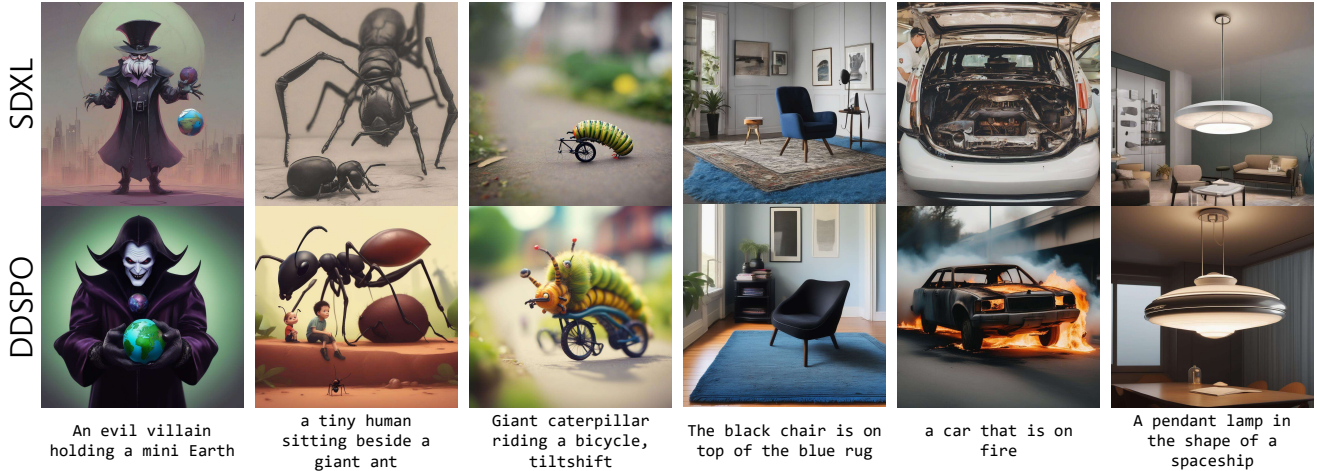


Figure 2. **Qualitative Comparison between SDXL and DDSPO.** Images are generated from the same prompts and random seeds.

Table 5. Effects of Various Prompt Perturbation Strategies. We compare different strategies for constructing dispreferred prompts to generate negative samples.

Method	T2I Alignment		Aesthetic Quality
	GE \uparrow	CB \uparrow	HPSv2 \uparrow
SD-1.4	.4245	.3150	26.88
Rand-removal	.5045	.3823	27.28
LLaMA (TA)	.4854	.3807	27.25
LLaMA (AQ)	.4758	.3616	27.51
			PickScore \uparrow

Table 6. Comparison of DDSPO with and without Explicit Negative Image Generation. We compare standard DDSPO with variants that avoid explicit negative image (NI) generation by reusing preferred samples with unpaired or perturbed prompts.

Method	NI generation	GenEval \uparrow	T2I-Compbench \uparrow
SD-1.4	-	.4245	.3150
Rand-removal	✓	.5045	.3823
Rand-positive	✗	.4866	.3763
Not-paired	✗	.4891	.3842

ously studied tasks. We evaluate three strategies: *Rand-removal*, which drops 40% to 70% of tokens from the original prompt; and *LLaMA*, which uses an LLM [10] to rewrite the prompt in a way that degrades task performance. The LLaMA-based strategy includes two task-specific variants: LLaMA (TA) for text-to-image alignment and LLaMA (AQ) for aesthetic quality improvement. When trained with DDSPO, we observe that Rand-removal yields the best performance on text-to-image alignment, while LLaMA (AQ) performs best for aesthetic quality improvement, as it is specifically tailored to that task.

Efficient DDSPO We introduce a data-efficient variant of DDSPO in which only preferred images \mathbf{x}_0^w are generated, without dispreferred ones \mathbf{x}_0^l , resulting in a dataset $\mathcal{D} = (\mathbf{x}_0^w, \mathbf{c})$ instead of $(\mathbf{x}_0^w, \mathbf{x}_0^l, \mathbf{c}, \mathbf{c}^-)$. To apply DDSPO

with \mathcal{D} , however, we still require a dispreferred sample \mathbf{x}_0^l to obtain its noisy version \mathbf{x}_t^l through the forward diffusion process, which is necessary to compute the dispreferred score ϵ_*^l . Following the technique described in Sec. 3.3, we randomly sample an image \mathbf{x}_0^+ from \mathcal{D} that was generated by a prompt unrelated to \mathbf{c} , and designate it as a pseudo-dispreferred image. Using this setup, we evaluate two perturbation strategies: Random-positive, which pairs the original prompt with a randomly selected image \mathbf{x}_0^+ ; and Not-paired, which uses a perturbed version of the original prompt (via random token removal) that is not strictly paired with the noised image \mathbf{x}_t^l . We compare these variants to the full setup that explicitly generates dispreferred images paired with perturbed prompts (Rand-Removal). As shown in Tab. 5, both Random-positive and Not-paired perform comparably to Rand-removal, where explicitly generated dispreferred samples are available. Interestingly, Not-paired outperforms Random-positive, despite using unpaired image–prompt combinations. These findings demonstrate that the negative direction in DDSPO can be effectively modeled from unpaired prompt–image instances, underscoring the framework’s flexibility in preference-signal modeling via stepwise supervision.

5. Conclusion

We introduce DDSPO, a novel preference optimization framework that extends Diffusion DPO by supervising each denoising step with preferred/dispreferred targets derived from winning and losing policies. In practice, we construct these targets label-free using prompt perturbations and a pretrained reference model, eliminating manual annotations and reward models. Our experiments show that DDSPO consistently improves text-image consistency and visual fidelity, offering a scalable and practical approach within the broader landscape of preference-based training methods.

References

[1] Kevin Black, Michael Janner, Yilun Du, Ilya Kostrikov, and Sergey Levine. Training diffusion models with reinforcement learning, 2024. 2

[2] Ralph Allan Bradley and Milton E. Terry. Rank analysis of incomplete block designs: I. the method of paired comparisons. *Biometrika*, 39(3/4):324–345, 1952. 3

[3] Xinyan Chen, Jiaxin Ge, Tianjun Zhang, Jiaming Liu, and Shanghang Zhang. Learning from mistakes: Iterative prompt relabeling for text-to-image diffusion model training. In *Findings of the Association for Computational Linguistics: EMNLP 2024*, pages 2937–2952, 2024. 2

[4] Kevin Clark, Paul Vicol, Kevin Swersky, and David J Fleet. Directly fine-tuning diffusion models on differentiable rewards. *arXiv preprint arXiv:2309.17400*, 2023. 2

[5] Florinel-Alin Croitoru, Vlad Hondu, Radu Tudor Ionescu, Nicu Sebe, and Mubarak Shah. Curriculum direct preference optimization for diffusion and consistency models. *arXiv preprint arXiv:2405.13637*, 2024. 2

[6] Yihe Deng, Pan Lu, Fan Yin, Ziniu Hu, Sheng Shen, Quanquan Gu, James Y Zou, Kai-Wei Chang, and Wei Wang. Enhancing large vision language models with self-training on image comprehension. *Advances in Neural Information Processing Systems*, 37:131369–131397, 2024. 2

[7] Ying Fan, Olivia Watkins, Yuqing Du, Hao Liu, Moonkyung Ryu, Craig Boutilier, Pieter Abbeel, Mohammad Ghavamzadeh, Kangwook Lee, and Kimin Lee. Dpok: Reinforcement learning for fine-tuning text-to-image diffusion models. *Advances in Neural Information Processing Systems*, 36:79858–79885, 2023. 2

[8] Golnaz Ghiasi, Barret Zoph, Ekin D Cubuk, Quoc V Le, and Tsung-Yi Lin. Multi-task self-training for learning general representations. In *2021 IEEE/CVF International Conference on Computer Vision (ICCV)*, pages 8836–8845. IEEE Computer Society, 2021. 2

[9] Dhruba Ghosh, Hannaneh Hajishirzi, and Ludwig Schmidt. Geneval: An object-focused framework for evaluating text-to-image alignment. *Advances in Neural Information Processing Systems*, 36:52132–52152, 2023. 6

[10] Aaron Grattafiori, Abhimanyu Dubey, Abhinav Jauhri, Abhinav Pandey, Abhishek Kadian, Ahmad Al-Dahle, Aiesha Letman, Akhil Mathur, Alan Schelten, Alex Vaughan, et al. The llama 3 herd of models. *arXiv preprint arXiv:2407.21783*, 2024. 7, 8, 21

[11] Yi Gu, Zhendong Wang, Yueqin Yin, Yujia Xie, and Mingyuan Zhou. Diffusion-rpo: Aligning diffusion models through relative preference optimization. *arXiv preprint arXiv:2406.06382*, 2024. 2

[12] Yaru Hao, Zewen Chi, Li Dong, and Furu Wei. Optimizing prompts for text-to-image generation. *Advances in Neural Information Processing Systems*, 36:66923–66939, 2023. 2

[13] Junxian He, Jiatao Gu, Jiajun Shen, and Marc’Aurelio Ranzato. Revisiting self-training for neural sequence generation. *arXiv preprint arXiv:1909.13788*, 2019. 2

[14] Martin Heusel, Hubert Ramsauer, Thomas Unterthiner, Bernhard Nessler, and Sepp Hochreiter. Gans trained by a two time-scale update rule converge to a local nash equilibrium. In *NeurIPS*, 2017. 6

[15] Jonathan Ho, Ajay Jain, and Pieter Abbeel. Denoising diffusion probabilistic models. In *Advances in Neural Information Processing Systems*, pages 6840–6851. Curran Associates, Inc., 2020. 1, 3, 12, 14

[16] Jiwoo Hong, Sayak Paul, Noah Lee, Kashif Rasul, James Thorne, and Jongheon Jeong. Margin-aware preference optimization for aligning diffusion models without reference. In *First Workshop on Scalable Optimization for Efficient and Adaptive Foundation Models*, 2025. 2, 7

[17] Edward J Hu, yelong shen, Phillip Wallis, Zeyuan Allen-Zhu, Yuanzhi Li, Shean Wang, Lu Wang, and Weizhu Chen. LoRA: Low-rank adaptation of large language models. In *International Conference on Learning Representations*, 2022. 19

[18] Kaiyi Huang, Kaiyue Sun, Enze Xie, Zhenguo Li, and Xihui Liu. T2i-compbench: A comprehensive benchmark for open-world compositional text-to-image generation. *Advances in Neural Information Processing Systems*, 36:78723–78747, 2023. 6, 19, 20

[19] Gi-Cheon Kang, Sungdong Kim, Jin-Hwa Kim, Donghyun Kwak, and Byoung-Tak Zhang. The dialog must go on: Improving visual dialog via generative self-training. In *2023 IEEE/CVF Conference on Computer Vision and Pattern Recognition (CVPR)*, pages 6746–6756. IEEE Computer Society, 2023. 2

[20] Tero Karras, Miika Aittala, Timo Aila, and Samuli Laine. Elucidating the design space of diffusion-based generative models. In *Advances in Neural Information Processing Systems*, 2022. 20

[21] Dohyun Kim, Sehwan Park, Geonhee Han, Seung Wook Kim, and Paul Hongsuck Seo. Random conditioning with distillation for data-efficient diffusion model compression. In *2025 IEEE/CVF Conference on Computer Vision and Pattern Recognition (CVPR)*, pages 18607–18618, 2025. 4

[22] Diederik Kingma, Tim Salimans, Ben Poole, and Jonathan Ho. Variational diffusion models. In *Advances in Neural Information Processing Systems*, pages 21696–21707. Curran Associates, Inc., 2021. 14

[23] Yuval Kirstain, Adam Polyak, Uriel Singer, Shahbuland Matiana, Joe Penna, and Omer Levy. Pick-a-pic: An open dataset of user preferences for text-to-image generation. In *Advances in Neural Information Processing Systems*, pages 36652–36663. Curran Associates, Inc., 2023. 2, 5, 7

[24] Jaa-Yeon Lee, Byunghee Cha, Jeongsol Kim, and Jong Chul Ye. Aligning text to image in diffusion models is easier than you think. *arXiv preprint arXiv:2503.08250*, 2025. 2

[25] Kyungmin Lee, Xiaohang Li, Qifei Wang, Junfeng He, Junjie Ke, Ming-Hsuan Yang, Irfan Essa, Jinwoo Shin, Feng Yang, and Yinxiao Li. Calibrated multi-preference optimization for aligning diffusion models. *arXiv preprint arXiv:2502.02588*, 2025. 2

[26] Kyungmin Lee, Xiaohang Li, Qifei Wang, Junfeng He, Junjie Ke, Ming-Hsuan Yang, Irfan Essa, Jinwoo Shin, Feng Yang, and Yinxiao Li. Calibrated multi-preference optimization for aligning diffusion models, 2025. 7, 20

[27] Junnan Li, Dongxu Li, Caiming Xiong, and Steven Hoi. Blip: Bootstrapping language-image pre-training for unified vision-language understanding and generation. In *ICML*, 2022. 20

[28] Shufan Li, Konstantinos Kallidromitis, Akash Gokul, Yusuke Kato, and Kazuki Kozuka. Aligning diffusion models by optimizing human utility. *arXiv preprint arXiv:2404.04465*, 2024. 2, 7

[29] Zhanhao Liang, Yuhui Yuan, Shuyang Gu, Bohan Chen, Tiankai Hang, Mingxi Cheng, Ji Li, and Liang Zheng. Aesthetic post-training diffusion models from generic preferences with step-by-step preference optimization, 2025. 2, 5, 7

[30] Tsung-Yi Lin, Michael Maire, Serge Belongie, James Hays, Pietro Perona, Deva Ramanan, Piotr Dollár, and C Lawrence Zitnick. Microsoft coco: Common objects in context. In *ECCV*, 2014. 6

[31] Yaron Lipman, Ricky T. Q. Chen, Heli Ben-Hamu, Maximilian Nickel, and Matthew Le. Flow matching for generative modeling. In *The Eleventh International Conference on Learning Representations*, 2023. 5

[32] Luping Liu, Yi Ren, Zhijie Lin, and Zhou Zhao. Pseudo numerical methods for diffusion models on manifolds. In *International Conference on Learning Representations*, 2022. 20

[33] Ziyu Liu, Yuhang Zang, Xiaoyi Dong, Pan Zhang, Yuhang Cao, Haodong Duan, Conghui He, Yuanjun Xiong, Dahua Lin, and Jiaqi Wang. Mia-dpo: Multi-image augmented direct preference optimization for large vision-language models. *arXiv preprint arXiv:2410.17637*, 2024. 2

[34] Ilya Loshchilov and Frank Hutter. Decoupled weight decay regularization. In *International Conference on Learning Representations*, 2017. 19

[35] Cheng Lu, Yuhao Zhou, Fan Bao, Jianfei Chen, Chongxuan Li, and Jun Zhu. Dpm-solver: A fast ode solver for diffusion probabilistic model sampling in around 10 steps. In *Advances in Neural Information Processing Systems*, pages 5775–5787. Curran Associates, Inc., 2022. 20

[36] Cheng Lu, Yuhao Zhou, Fan Bao, Jianfei Chen, Chongxuan Li, and Jun Zhu. Dpm-solver++: Fast solver for guided sampling of diffusion probabilistic models. *arXiv preprint arXiv:2211.01095*, 2022. 20

[37] Navonil Majumder, Chia-Yu Hung, Deepanway Ghosal, Wei-Ning Hsu, Rada Mihalcea, and Soujanya Poria. Tango 2: Aligning diffusion-based text-to-audio generative models through direct preference optimization. In *ACM Multimedia 2024*, 2024. 2

[38] Dustin Podell, Zion English, Kyle Lacey, Andreas Blattmann, Tim Dockhorn, Jonas Müller, Joe Penna, and Robin Rombach. SDXL: Improving latent diffusion models for high-resolution image synthesis. In *The Twelfth International Conference on Learning Representations*, 2024. 1, 7, 18, 19

[39] Mihir Prabhudesai, Anirudh Goyal, Deepak Pathak, and Katerina Fragkiadaki. Aligning text-to-image diffusion models with reward backpropagation. *arXiv preprint arXiv:2310.03739*, 2023. 2

[40] Alec Radford, Jong Wook Kim, Chris Hallacy, Aditya Ramesh, Gabriel Goh, Sandhini Agarwal, Girish Sastry, Amanda Askell, Pamela Mishkin, Jack Clark, Gretchen Krueger, and Ilya Sutskever. Learning transferable visual models from natural language supervision. In *Proceedings of the 38th International Conference on Machine Learning*, pages 8748–8763. PMLR, 2021. 20

[41] Rafael Rafailov, Archit Sharma, Eric Mitchell, Christopher D Manning, Stefano Ermon, and Chelsea Finn. Direct preference optimization: Your language model is secretly a reward model. *Advances in Neural Information Processing Systems*, 36:53728–53741, 2023. 1, 2, 12

[42] Aditya Ramesh, Prafulla Dhariwal, Alex Nichol, Casey Chu, and Mark Chen. Hierarchical text-conditional image generation with clip latents. *ArXiv*, abs/2204.06125, 2022. 1

[43] Robin Rombach and Patrick Esser. Stable diffusion v1-4. <https://huggingface.co/CompVis/stable-diffusion-v1-4>, 2022. 6, 7, 19

[44] Robin Rombach and Patrick Esser. Stable diffusion v1-5. <https://huggingface.co/stable-diffusion-v1-5/stable-diffusion-v1-5>, 2022. 1, 7, 19

[45] Robin Rombach, Andreas Blattmann, Dominik Lorenz, Patrick Esser, and Björn Ommer. High-resolution image synthesis with latent diffusion models. In *Proceedings of the IEEE/CVF Conference on Computer Vision and Pattern Recognition (CVPR)*, pages 10684–10695, 2022. 1

[46] Chitwan Saharia, William Chan, Saurabh Saxena, Lala Li, Jay Whang, Emily Denton, Seyed Kamyar Seyed Ghasemipour, Raphael Gontijo-Lopes, Burcu Karagol Ayan, Tim Salimans, Jonathan Ho, David J. Fleet, and Mohammad Norouzi. Photorealistic text-to-image diffusion models with deep language understanding. In *Advances in Neural Information Processing Systems*, 2022. 1

[47] Tim Salimans, Ian Goodfellow, Wojciech Zaremba, Vicki Cheung, Alec Radford, and Xi Chen. Improved techniques for training gans. In *NeurIPS*, 2016. 6, 19

[48] Noam Shazeer and Mitchell Stern. Adafactor: Adaptive learning rates with sublinear memory cost. In *Proceedings of the 35th International Conference on Machine Learning*, pages 4596–4604. PMLR, 2018. 19

[49] Jascha Sohl-Dickstein, Eric Weiss, Niru Maheswaranathan, and Surya Ganguli. Deep unsupervised learning using nonequilibrium thermodynamics. In *International conference on machine learning*, pages 2256–2265, 2015. 12

[50] Kihyuk Sohn, David Berthelot, Nicholas Carlini, Zizhao Zhang, Han Zhang, Colin A Raffel, Ekin Dogus Cubuk, Alexey Kurakin, and Chun-Liang Li. Fixmatch: Simplifying semi-supervised learning with consistency and confidence. *Advances in neural information processing systems*, 33:596–608, 2020. 2

[51] Yang Song, Jascha Sohl-Dickstein, Diederik P Kingma, Abhishek Kumar, Stefano Ermon, and Ben Poole. Score-based generative modeling through stochastic differential equations. In *International Conference on Learning Representations*, 2021. 3, 4, 12

[52] Bram Wallace, Meihua Dang, Rafael Rafailov, Linqi Zhou, Aaron Lou, Senthil Purushwalkam, Stefano Ermon, Caiming

Xiong, Shafiq Joty, and Nikhil Naik. Diffusion model alignment using direct preference optimization. In *Proceedings of the IEEE/CVF Conference on Computer Vision and Pattern Recognition (CVPR)*, pages 8228–8238, 2024. 1, 2, 3, 6, 7, 16, 19

[53] Zijie J. Wang, Evan Montoya, David Munechika, Haoyang Yang, Benjamin Hoover, and Duen Horng Chau. DiffusionDB: A large-scale prompt gallery dataset for text-to-image generative models. *arXiv:2210.14896 [cs]*, 2022. 6

[54] Colin Wei, Kendrick Shen, Yining Chen, and Tengyu Ma. Theoretical analysis of self-training with deep networks on unlabeled data. *arXiv preprint arXiv:2010.03622*, 2020. 2

[55] Xiaoshi Wu, Yiming Hao, Keqiang Sun, Yixiong Chen, Feng Zhu, Rui Zhao, and Hongsheng Li. Human preference score v2: A solid benchmark for evaluating human preferences of text-to-image synthesis. *arXiv preprint arXiv:2306.09341*, 2023. 7

[56] Enze Xie, Junsong Chen, Junyu Chen, Han Cai, Haotian Tang, Yujun Lin, Zhekai Zhang, Muyang Li, Ligeng Zhu, Yao Lu, et al. Sana: Efficient high-resolution image synthesis with linear diffusion transformers. *arXiv preprint arXiv:2410.10629*, 2024. 5, 7, 19

[57] Qizhe Xie, Minh-Thang Luong, Eduard Hovy, and Quoc V Le. Self-training with noisy student improves imagenet classification. In *Proceedings of the IEEE/CVF conference on computer vision and pattern recognition*, pages 10687–10698, 2020. 2

[58] Yuxi Xie, Guanzhen Li, Xiao Xu, and Min-Yen Kan. V-dpo: Mitigating hallucination in large vision language models via vision-guided direct preference optimization. In *Findings of the Association for Computational Linguistics: EMNLP 2024*, pages 13258–13273, 2024. 1

[59] Shuo Xing, Yuping Wang, Peiran Li, Ruizheng Bai, Yueqi Wang, Chengxuan Qian, Huaxiu Yao, and Zhengzhong Tu. Re-align: Aligning vision language models via retrieval-augmented direct preference optimization. *arXiv preprint arXiv:2502.13146*, 2025. 1, 2

[60] Jiazheng Xu, Xiao Liu, Yuchen Wu, Yuxuan Tong, Qinkai Li, Ming Ding, Jie Tang, and Yuxiao Dong. Imagereward: Learning and evaluating human preferences for text-to-image generation. *Advances in Neural Information Processing Systems*, 36:15903–15935, 2023. 2

[61] Kai Yang, Jian Tao, Jiafei Lyu, Chunjiang Ge, Jiaxin Chen, Qimai Li, Weihan Shen, Xiaolong Zhu, and Xiu Li. Using human feedback to fine-tune diffusion models without any reward model, 2024. 2

[62] Jiahui Yu, Yuanzhong Xu, Jing Yu Koh, Thang Luong, Gunjan Baid, Zirui Wang, Vijay Vasudevan, Alexander Ku, Yinfei Yang, Burcu Karagol Ayan, et al. Scaling autoregressive models for content-rich text-to-image generation. *Transactions on Machine Learning Research*, 2022. 7

[63] Huizhuo Yuan, Zixiang Chen, Kaixuan Ji, and Quanquan Gu. Self-play fine-tuning of diffusion models for text-to-image generation. *arXiv preprint arXiv:2402.10210*, 2024. 2

[64] Xinchen Zhang, Ling Yang, Guohao Li, YaQi Cai, xie jiake, Yong Tang, Yujiu Yang, Mengdi Wang, and Bin CUI. Iter-comp: Iterative composition-aware feedback learning from model gallery for text-to-image generation. In *The Thirteenth International Conference on Learning Representations*, 2025. 2, 5, 7

[65] Ziyi Zhang, Li Shen, Sen Zhang, Deheng Ye, Yong Luo, Miaojing Shi, Bo Du, and Dacheng Tao. Aligning few-step diffusion models with dense reward difference learning. *arXiv preprint arXiv:2411.11727*, 2024. 2

[66] Hanyang Zhao, Haoxian Chen, Yucheng Guo, Genta Indra Winata, Tingting Ou, Ziyu Huang, David D Yao, and Wenpin Tang. Fine-tuning diffusion generative models via rich preference optimization. *arXiv preprint arXiv:2503.11720*, 2025. 2

[67] Xingyi Zhou, Vladlen Koltun, and Philipp Krähenbühl. Simple multi-dataset detection. In *Proceedings of the IEEE/CVF Conference on Computer Vision and Pattern Recognition (CVPR)*, pages 7571–7580, 2022. 20

[68] Huaisheng Zhu, Teng Xiao, and Vasant G Honavar. Dspo: Direct score preference optimization for diffusion model alignment. In *The Thirteenth International Conference on Learning Representations*, 2025. 2, 5, 6, 15

[69] Ke Zhu, Liang Zhao, Zheng Ge, and Xiangyu Zhang. Self-supervised visual preference alignment. In *Proceedings of the 32nd ACM International Conference on Multimedia*, pages 291–300, 2024. 2

[70] Barret Zoph, Golnaz Ghiasi, Tsung-Yi Lin, Yin Cui, Hanxiao Liu, Ekin Dogus Cubuk, and Quoc Le. Rethinking pre-training and self-training. *Advances in neural information processing systems*, 33:3833–3845, 2020. 2

Direct Diffusion Score Preference Optimization via Stepwise Contrastive Policy-Pair Supervision

supplementary material

A. Derivation

Diffusion Model Denoising diffusion probabilistic models [15, 49, 51] define a generative process that reverses a fixed forward noising process applied to data drawn from $q(\mathbf{x}_0)$. This reverse process is modeled as a discrete-time Markov chain over latent variables $\mathbf{x}_{0:T}$, with the joint distribution defined as $p_\theta(\mathbf{x}_{0:T}) = p(\mathbf{x}_T) \prod_{t=1}^T p_\theta(\mathbf{x}_{t-1} \mid \mathbf{x}_t)$. Each transition $p_\theta(\mathbf{x}_{t-1} \mid \mathbf{x}_t)$ is modeled as a Gaussian distribution:

$$p_\theta(\mathbf{x}_{t-1} \mid \mathbf{x}_t) = \mathcal{N}(\mathbf{x}_{t-1}; \mu_\theta(\mathbf{x}_t), \sigma_{t|t-1}^2 \frac{\sigma_{t-1}^2}{\sigma_t^2} \mathbf{I}). \quad (7)$$

During training, the model is optimized to approximate the true reverse process by minimizing a variational bound on the negative log-likelihood. In practice, this reduces to predicting the noise ϵ added at each timestep, leading to a simplified objective of the form:

$$\mathcal{L}_{\text{MSE}} = \mathbb{E}_{t, \mathbf{x}_0, \epsilon \sim \mathcal{N}(0, I)} \left[\|\epsilon - \epsilon_\theta(\mathbf{x}_t, t)\|_2^2 \right], \quad (8)$$

where $\mathbf{x}_t = \sqrt{\alpha_t} \mathbf{x}_0 + \sqrt{1 - \alpha_t} \epsilon$ is the noised sample at timestep t , and ϵ_θ is the model's prediction of the noise.

Direct Preference Optimization In Eq. (1), reward model $r(\mathbf{c}, \mathbf{x}_0^w)$ can be parameterized by a neural net work ϕ and estimated via maximum likelihood training for binary classification:

$$L_{\text{BT}}(\phi) = -\mathbb{E}_{\mathbf{c}, \mathbf{x}_0^w, \mathbf{x}_0^l} [\log \sigma(r_\phi(\mathbf{c}, \mathbf{x}_0^w) - r_\phi(\mathbf{c}, \mathbf{x}_0^l))] \quad (9)$$

And in RLHF objective Eq. (2), the unique global optimal solution p_θ^* takes the form:

$$p_\theta^*(\mathbf{x}_0 \mid \mathbf{c}) = p_{\text{ref}}(\mathbf{x}_0 \mid \mathbf{c}) \exp(r(\mathbf{c}, \mathbf{x}_0) / \beta) / Z(\mathbf{c}) \quad (10)$$

where $Z(\mathbf{c}) = \sum_{\mathbf{x}_0} p_{\text{ref}}(\mathbf{x}_0 \mid \mathbf{c}) \exp(r(\mathbf{c}, \mathbf{x}_0) / \beta)$ is the partition function. Hence, the reward function is rewritten as

$$r(\mathbf{c}, \mathbf{x}_0) = \beta \log \frac{p_\theta^*(\mathbf{x}_0 \mid \mathbf{c})}{p_{\text{ref}}(\mathbf{x}_0 \mid \mathbf{c})} + \beta \log Z(\mathbf{c}) \quad (11)$$

Using Eq. (9) the reward objective becomes:

$$L_{\text{DPO}}(\theta) = -\mathbb{E}_{\mathbf{c}, \mathbf{x}_0^w, \mathbf{x}_0^l} \left[\log \sigma \left(\beta \log \frac{p_\theta(\mathbf{x}_0^w \mid \mathbf{c})}{p_{\text{ref}}(\mathbf{x}_0^w \mid \mathbf{c})} - \beta \log \frac{p_\theta(\mathbf{x}_0^l \mid \mathbf{c})}{p_{\text{ref}}(\mathbf{x}_0^l \mid \mathbf{c})} \right) \right] \quad (12)$$

By this reparameterization, instead of optimizing the reward function r_ϕ and then performing RL, [41] directly optimizes the optimal conditional distribution $p_\theta(\mathbf{x}_0 \mid \mathbf{c})$.

Diffusion DPO Diffusion DPO extend the DPO formulation to diffusion models by defining the reward function over full denoising trajectories. Specifically, they assume that the reward is given by the expected trajectory-level score:

$$r(\mathbf{c}, \mathbf{x}_0) = \mathbb{E}_{p_\theta(\mathbf{x}_{1:T} \mid \mathbf{x}_0, \mathbf{c})} [R(\mathbf{c}, \mathbf{x}_{0:T})]. \quad (13)$$

Under this definition, the RLHF objective from Eq. (2) can be reformulated as:

$$\max_{p_\theta} \mathbb{E}_{\mathbf{c} \sim \mathcal{D}_c, \mathbf{x}_{0:T} \sim p_\theta(\mathbf{x}_{0:T} \mid \mathbf{c})} [r(\mathbf{c}, \mathbf{x}_0)] - \beta \mathbb{D}_{\text{KL}} [p_\theta(\mathbf{x}_{0:T} \mid \mathbf{c}) \parallel p_{\text{ref}}(\mathbf{x}_{0:T} \mid \mathbf{c})]. \quad (14)$$

Similar with Eq. (10), the optimal policy $p_\theta^*(\mathbf{x}_{0:T}|\mathbf{c})$ has a unique closed-form solution:

$$p_\theta^*(\mathbf{x}_{0:T}|\mathbf{c}) = p_{\text{ref}}(\mathbf{x}_{0:T}|\mathbf{c}) \exp(R(\mathbf{c}, \mathbf{x}_{0:T})/\beta)/Z(\mathbf{c}), \quad (15)$$

where $Z(\mathbf{c}) = \sum_{\mathbf{x}} p_{\text{ref}}(\mathbf{x}_{0:T}|\mathbf{c}) \exp(r(\mathbf{c}, \mathbf{x}_0)/\beta)$ is the partition function. The reparameterized form of the trajectory-level reward is given by

$$R(\mathbf{c}, \mathbf{x}_{0:T}) = \beta \log \frac{p_\theta^*(\mathbf{x}_{0:T}|\mathbf{c})}{p_{\text{ref}}(\mathbf{x}_{0:T}|\mathbf{c})} + \beta \log Z(\mathbf{c}). \quad (16)$$

Inserting this expression into the definition of $r(\mathbf{c}, \mathbf{x}_0)$ Eq. (13) leads to

$$r(\mathbf{c}, \mathbf{x}_0) = \beta \mathbb{E}_{p_\theta(\mathbf{x}_{1:T}|\mathbf{x}_0, \mathbf{c})} \left[\log \frac{p_\theta^*(\mathbf{x}_{0:T}|\mathbf{c})}{p_{\text{ref}}(\mathbf{x}_{0:T}|\mathbf{c})} \right] + \beta \log Z(\mathbf{c}).$$

Substituting the resulting reward into the Bradley–Terry objective Eq. (9) yields a maximum likelihood formulation for diffusion models. Since the partition function cancels in the pairwise setting, the per-example loss becomes:

$$L_{\text{Diffusion-DPO}}(\theta) = -\log \sigma \left(\beta \mathbb{E}_{\mathbf{x}_{1:T}^w \sim p_\theta(\mathbf{x}_{1:T}|\mathbf{x}_0^w, \mathbf{c}), \mathbf{x}_{1:T}^l \sim p_\theta(\mathbf{x}_{1:T}^l|\mathbf{x}_0^l, \mathbf{c})} \left[\log \frac{p_\theta(\mathbf{x}_{0:T}^w|\mathbf{c})}{p_{\text{ref}}(\mathbf{x}_{0:T}^w|\mathbf{c})} - \log \frac{p_\theta(\mathbf{x}_{0:T}^l|\mathbf{c})}{p_{\text{ref}}(\mathbf{x}_{0:T}^l|\mathbf{c})} \right] \right) \quad (17)$$

Here, \mathbf{x}_0^w and \mathbf{x}_0^l are drawn from a static dataset, and the conditioning input \mathbf{c} is omitted for clarity.

To address the intractability of directly sampling from the true reverse process $p_\theta(\mathbf{x}_{1:T}|\mathbf{x}_0)$, the Diffusion DPO formulation approximates it using the forward posterior $q(\mathbf{x}_{1:T}|\mathbf{x}_0)$. Under this approximation, the trajectory-level preference objective can be rewritten as an expectation over individual timesteps. Specifically, comparisons between full trajectories are expressed as averages over comparisons between corresponding reverse transitions at each timestep, yielding the following expression:

$$L_{\text{Diffusion-DPO}}(\theta) = -\log \sigma \left(\beta T \mathbb{E}_t \mathbb{E}_{\mathbf{x}_{t-1,t}^w \sim q(\mathbf{x}_{t-1,t}|\mathbf{x}_0^w), \mathbf{x}_{t-1,t}^l \sim q(\mathbf{x}_{t-1,t}|\mathbf{x}_0^l)} \left[\log \frac{p_\theta(\mathbf{x}_{t-1}^w|\mathbf{x}_t^w, \mathbf{c})}{p_{\text{ref}}(\mathbf{x}_{t-1}^w|\mathbf{x}_t^w, \mathbf{c})} - \log \frac{p_\theta(\mathbf{x}_{t-1}^l|\mathbf{x}_t^l, \mathbf{c})}{p_{\text{ref}}(\mathbf{x}_{t-1}^l|\mathbf{x}_t^l, \mathbf{c})} \right] \right) \quad (18)$$

To derive a tractable approximation, Jensen's inequality is applied to move the logarithm outside the expectation, yielding an upper bound on the original loss:

$$\begin{aligned} L_{\text{Diffusion-DPO}}(\theta) &\leq -\mathbb{E}_{t, \mathbf{x}_t^w \sim q(\mathbf{x}_t|\mathbf{x}_0^w), \mathbf{x}_t^l \sim q(\mathbf{x}_t|\mathbf{x}_0^l)} \log \sigma \left(\beta T \cdot \right. \\ &\quad \mathbb{E}_{\mathbf{x}_{t-1}^w \sim q(\mathbf{x}_{t-1}|\mathbf{x}_t^w, \mathbf{x}_0^w), \mathbf{x}_{t-1}^l \sim q(\mathbf{x}_{t-1}|\mathbf{x}_t^l, \mathbf{x}_0^l)} \left[\log \frac{p_\theta(\mathbf{x}_{t-1}^w|\mathbf{x}_t^w, \mathbf{c})}{p_{\text{ref}}(\mathbf{x}_{t-1}^w|\mathbf{x}_t^w, \mathbf{c})} - \log \frac{p_\theta(\mathbf{x}_{t-1}^l|\mathbf{x}_t^l, \mathbf{c})}{p_{\text{ref}}(\mathbf{x}_{t-1}^l|\mathbf{x}_t^l, \mathbf{c})} \right] \\ &= -\mathbb{E}_{t, \mathbf{x}_t^w \sim q(\mathbf{x}_t|\mathbf{x}_0^w), \mathbf{x}_t^l \sim q(\mathbf{x}_t|\mathbf{x}_0^l)} \log \sigma \left(\beta T \cdot \right. \\ &\quad \mathbb{E}_{\mathbf{x}_{t-1}^w \sim q(\mathbf{x}_{t-1}|\mathbf{x}_t^w, \mathbf{x}_0^w), \mathbf{x}_{t-1}^l \sim q(\mathbf{x}_{t-1}|\mathbf{x}_t^l, \mathbf{x}_0^l)} \left[\log \frac{p_\theta(\mathbf{x}_{t-1}^w|\mathbf{x}_0^w, \mathbf{c})}{q(\mathbf{x}_{t-1}^w|\mathbf{x}_0^w)} - \log \frac{q(\mathbf{x}_{t-1}^l|\mathbf{x}_0^w)}{p_{\text{ref}}(\mathbf{x}_{t-1}^l|\mathbf{x}_0^w, \mathbf{c})} \right. \\ &\quad \left. \left. - \left(\log \frac{p_\theta(\mathbf{x}_{t-1}^l|\mathbf{x}_t^l, \mathbf{c})}{q(\mathbf{x}_{t-1}^l|\mathbf{x}_0^l)} - \log \frac{q(\mathbf{x}_{t-1}^l|\mathbf{x}_0^l)}{p_{\text{ref}}(\mathbf{x}_{t-1}^l|\mathbf{x}_t^l, \mathbf{c})} \right) \right] \right) \\ &= -\mathbb{E}_{t, \mathbf{x}_t^w \sim q(\mathbf{x}_t|\mathbf{x}_0^w), \mathbf{x}_t^l \sim q(\mathbf{x}_t|\mathbf{x}_0^l)} \log \sigma \left(-\beta T \cdot \right. \\ &\quad \mathbb{D}_{\text{KL}} \left(q(\mathbf{x}_{t-1}^w|\mathbf{x}_0^w) \parallel p_\theta(\mathbf{x}_{t-1}^w|\mathbf{x}_t^w, \mathbf{c}) \right) - \mathbb{D}_{\text{KL}} \left(q(\mathbf{x}_{t-1}^l|\mathbf{x}_0^w) \parallel p_{\text{ref}}(\mathbf{x}_{t-1}^l|\mathbf{x}_t^w, \mathbf{c}) \right) \\ &\quad \left. - \left(\mathbb{D}_{\text{KL}} \left(q(\mathbf{x}_{t-1}^l|\mathbf{x}_0^l) \parallel p_\theta(\mathbf{x}_{t-1}^l|\mathbf{x}_t^l, \mathbf{c}) \right) - \mathbb{D}_{\text{KL}} \left(q(\mathbf{x}_{t-1}^l|\mathbf{x}_0^l) \parallel p_{\text{ref}}(\mathbf{x}_{t-1}^l|\mathbf{x}_t^l, \mathbf{c}) \right) \right) \right) \end{aligned} \quad (19)$$

Using the Gaussian parameterization of the reverse process (Eq. (7)), the above loss simplifies to:

$$L_{\text{Diffusion-DPO}}(\theta) \leq -\mathbb{E}_{(\mathbf{x}_0^w, \mathbf{x}_0^l) \sim \mathcal{D}, t \sim \mathcal{U}(0, T), \mathbf{x}_t^w \sim q(\mathbf{x}_t^w | \mathbf{x}_0^w), \mathbf{x}_t^l \sim q(\mathbf{x}_t^l | \mathbf{x}_0^l)} \log \sigma \left(-\beta \cdot [\right. \\ \left. \|\boldsymbol{\epsilon}^w - \boldsymbol{\epsilon}_\theta(\mathbf{x}_t^w, t, \mathbf{c})\|_2^2 - \|\boldsymbol{\epsilon}^w - \boldsymbol{\epsilon}_{\text{ref}}(\mathbf{x}_t^w, t, \mathbf{c})\|_2^2 - (\|\boldsymbol{\epsilon}^l - \boldsymbol{\epsilon}_\theta(\mathbf{x}_t^l, t, \mathbf{c})\|_2^2 - \|\boldsymbol{\epsilon}^l - \boldsymbol{\epsilon}_{\text{ref}}(\mathbf{x}_t^l, t, \mathbf{c})\|_2^2)] \right)$$

where $\boldsymbol{\epsilon}^w, \boldsymbol{\epsilon}^l \sim \mathcal{N}(0, I)$, $\mathbf{x}_t \sim q(\mathbf{x}_t | \mathbf{x}_0)$ thus $\mathbf{x}_t = \alpha_t \mathbf{x}_0 + \sigma_t \boldsymbol{\epsilon}$. $\lambda_t = \alpha_t^2 / \sigma_t^2$ is a signal-to-noise ratio term [22], in practice, the reweighting assigns each term the same weight [15].

DDSPO The DDSPO objective reformulates preference supervision in the diffusion framework by focusing on intermediate denoising transitions rather than final samples. Unlike standard DPO, which defines preferences over terminal outputs $(\mathbf{x}_0^w, \mathbf{x}_0^l | \mathbf{c})$, the DDSPO formulation assumes supervision over denoising transitions $((\mathbf{x}_t^w, \mathbf{x}_{t-1}^w), (\mathbf{x}_t^l, \mathbf{x}_{t-1}^l) | \mathbf{c})$ at arbitrary timesteps t .

Let $p_*^w(\mathbf{x}_{t-1,t} | \mathbf{c})$ and $p_*^l(\mathbf{x}_{t-1,t} | \mathbf{c})$ denote preferred and dispreferred denoising distributions respectively, conditioned on prompt \mathbf{c} . Following the Bradley–Terry approach in Eq. (9), the reward is redefined over denoising transitions as a function $r(\mathbf{c}, \mathbf{x}_t, \mathbf{x}_{t-1})$, with preference assigned to transitions sampled from p_*^w over those from p_*^l .

In this formulation, preference over transitions can be modeled analogously to Eq. (1), by replacing the reward function over final samples $r(\mathbf{c}, \mathbf{x}_0)$ with a reward function over transitions $r(\mathbf{c}, \mathbf{x}_t, \mathbf{x}_{t-1})$:

$$\mathbb{P}((\mathbf{x}_t^w, \mathbf{x}_{t-1}^w) \succ (\mathbf{x}_t^l, \mathbf{x}_{t-1}^l) | \mathbf{c}) = \sigma(r(\mathbf{c}, \mathbf{x}_t^w, \mathbf{x}_{t-1}^w) - r(\mathbf{c}, \mathbf{x}_t^l, \mathbf{x}_{t-1}^l)), \quad (20)$$

Similar to Eq. (9), the reward model $r(\mathbf{c}, \mathbf{x}_t, \mathbf{x}_{t-1})$ can be parameterized by a neural network ϕ , and trained using maximum likelihood estimation for binary classification:

$$L_{\text{BT}}(\phi) = -\mathbb{E}_{\mathbf{c}, \mathbf{x}_{t-1}^w, \mathbf{x}_t^w, \mathbf{x}_{t-1}^l, \mathbf{x}_t^l} [\log \sigma(r_\phi(\mathbf{c}, \mathbf{x}_t^w, \mathbf{x}_{t-1}^w) - r_\phi(\mathbf{c}, \mathbf{x}_t^l, \mathbf{x}_{t-1}^l))] \quad (21)$$

This contrasts with standard DPO or Diffusion DPO, where preference pairs $(\mathbf{x}_0^w, \mathbf{x}_0^l | \mathbf{c})$ are drawn from a dataset \mathcal{D} of full samples. In DDSPO, supervision instead arises from tuples $((\mathbf{x}_t^w, \mathbf{x}_{t-1}^w), (\mathbf{x}_t^l, \mathbf{x}_{t-1}^l) | \mathbf{c})$ sampled from preferred and dispreferred denoising policies $p_*^w(\mathbf{x}_{t-1,t} | \mathbf{c})$ and $p_*^l(\mathbf{x}_{t-1,t} | \mathbf{c})$. This allows DDSPO to directly optimize the model’s denoising behavior at each timestep t , rather than the distribution over final outputs. This formulation enables a direct comparison between denoising transitions at the same timestep, providing fine-grained supervision over the reverse process.

Accordingly, the DDSPO objective adopts a DPO-style structure defined over transitions, analogous to Eq. (2):

$$\max_{p_\theta} \mathbb{E}_{\mathbf{c}, \mathbf{x}_{t-1,t} \sim p_\theta(\mathbf{x}_{t-1,t} | \mathbf{c})} [r(\mathbf{c}, \mathbf{x}_t, \mathbf{x}_{t-1})] - \beta \mathbb{D}_{\text{KL}} [p_\theta(\mathbf{x}_{t-1} | \mathbf{x}_t, \mathbf{c}) \| p_{\text{ref}}(\mathbf{x}_{t-1} | \mathbf{x}_t, \mathbf{c})] \quad (22)$$

The optimal reverse transition distribution under this formulation has the form:

$$p_\theta^*(\mathbf{x}_{t-1} | \mathbf{x}_t, \mathbf{c}) = p_{\text{ref}}(\mathbf{x}_{t-1} | \mathbf{x}_t, \mathbf{c}) \cdot \frac{\exp(r(\mathbf{c}, \mathbf{x}_t, \mathbf{x}_{t-1}) / \beta)}{Z(\mathbf{c})}, \quad (23)$$

where the partition function $Z(\mathbf{c})$ is defined as

$$Z(\mathbf{c}) = \sum_{\mathbf{x}_t, \mathbf{x}_{t-1}} p_{\text{ref}}(\mathbf{x}_{t-1} | \mathbf{x}_t, \mathbf{c}) \exp(r(\mathbf{c}, \mathbf{x}_t, \mathbf{x}_{t-1}) / \beta).$$

The reward can thus be reparameterized as

$$r(\mathbf{c}, \mathbf{x}_t, \mathbf{x}_{t-1}) = \beta \log \frac{p_\theta^*(\mathbf{x}_{t-1} | \mathbf{x}_t, \mathbf{c})}{p_{\text{ref}}(\mathbf{x}_{t-1} | \mathbf{x}_t, \mathbf{c})} + \beta \log Z(\mathbf{c}). \quad (24)$$

Substituting the reward expression from Eq. (24) into the Bradley–Terry objective Eq. (21) yields a per-example loss defined over denoising transitions:

$$\ell_{\text{DDSPO}}^{(t)}(\theta) = \mathbb{E}_{\mathbf{c} \sim \mathcal{D}(\mathbf{c}), (\mathbf{x}_{t-1}^w, \mathbf{x}_t^w) \sim p_*^w(\mathbf{x}_{t-1,t}^w | \mathbf{c}), (\mathbf{x}_{t-1}^l, \mathbf{x}_t^l) \sim p_*^l(\mathbf{x}_{t-1,t}^l | \mathbf{c})} \left[-\log \sigma \left(\beta \log \frac{p_\theta(\mathbf{x}_{t-1}^w | \mathbf{x}_t^w, \mathbf{c})}{p_{\text{ref}}(\mathbf{x}_{t-1}^w | \mathbf{x}_t^w, \mathbf{c})} - \beta \log \frac{p_\theta(\mathbf{x}_{t-1}^l | \mathbf{x}_t^l, \mathbf{c})}{p_{\text{ref}}(\mathbf{x}_{t-1}^l | \mathbf{x}_t^l, \mathbf{c})} \right) \right] \quad (25)$$

The full DDSPO objective is then obtained by taking the expectation over uniformly sampled timesteps $t \sim \mathcal{U}(0, T)$. Equivalently, this corresponds to uniformly averaging per-timestep losses across all diffusion steps:

$$\mathcal{L}_{\text{DDSPO}}(\theta) = \mathbb{E}_{t \sim \mathcal{U}(0, T)} \left[\ell_{\text{DDSPO}}^{(t)}(\theta) \right], \quad (26)$$

Concretely, we instantiate it as:

$$\begin{aligned} \mathcal{L}_{\text{DDSPO}}(\theta) = & -\mathbb{E}_{\mathbf{c} \sim \mathcal{D}(c), t \sim \mathcal{U}(0, T), (\mathbf{x}_{t-1}^w, \mathbf{x}_t^w) \sim p_{\star}^w(\mathbf{x}_{t-1}^w | \mathbf{c}), (\mathbf{x}_{t-1}^l, \mathbf{x}_t^l) \sim p_{\star}^l(\mathbf{x}_{t-1}^l | \mathbf{c})} \\ & \log \sigma \left(\beta \log \frac{p_{\theta}(\mathbf{x}_{t-1}^w | \mathbf{x}_t^w, \mathbf{c})}{p_{\text{ref}}(\mathbf{x}_{t-1}^w | \mathbf{x}_t^w, \mathbf{c})} - \beta \log \frac{p_{\theta}(\mathbf{x}_{t-1}^l | \mathbf{x}_t^l, \mathbf{c})}{p_{\text{ref}}(\mathbf{x}_{t-1}^l | \mathbf{x}_t^l, \mathbf{c})} \right) \end{aligned}$$

As in Diffusion DPO, we approximate the intractable joint transition distribution

$$p_{\star}^w(\mathbf{x}_{t-1}^w | c) \approx q(\mathbf{x}_t^w | \mathbf{x}_0^w) \cdot p_{\star}(\mathbf{x}_{t-1}^w | \mathbf{x}_t^w, c), \quad (27)$$

where $\mathbf{x}_0^w \sim \mathcal{D}$, $\mathbf{x}_t^w \sim q(\mathbf{x}_t^w | \mathbf{x}_0^w)$, and $\mathbf{x}_{t-1}^w \sim p_{\star}(\mathbf{x}_{t-1}^w | \mathbf{x}_t^w, c)$. The same applies to the dispreferred trajectory $(\mathbf{x}_t^l, \mathbf{x}_{t-1}^l)$.

Substituting this into the DDSPO objective yields:

$$\begin{aligned} \mathcal{L}_{\text{DDSPO}}(\theta) = & \mathbb{E}_{\mathbf{c} \sim \mathcal{D}(c), t \sim \mathcal{U}(0, T), (\mathbf{x}_{t-1}^w, \mathbf{x}_t^w) \sim q(\mathbf{x}_t^w | \mathbf{x}_0^w) \cdot p_{\star}^w(\mathbf{x}_{t-1}^w | \mathbf{x}_t^w, c), (\mathbf{x}_{t-1}^l, \mathbf{x}_t^l) \sim q(\mathbf{x}_t^l | \mathbf{x}_0^l) \cdot p_{\star}^l(\mathbf{x}_{t-1}^l | \mathbf{x}_t^l, c)} \\ & \left[-\log \sigma \left(\beta \log \frac{p_{\theta}(\mathbf{x}_{t-1}^w | \mathbf{x}_t^w, c)}{p_{\text{ref}}(\mathbf{x}_{t-1}^w | \mathbf{x}_t^w, c)} - \beta \log \frac{p_{\theta}(\mathbf{x}_{t-1}^l | \mathbf{x}_t^l, c)}{p_{\text{ref}}(\mathbf{x}_{t-1}^l | \mathbf{x}_t^l, c)} \right) \right] \\ \leq & -\mathbb{E}_{\mathbf{c} \sim \mathcal{D}(c), t \sim \mathcal{U}(0, T), \mathbf{x}_t^w \sim q(\mathbf{x}_t^w | \mathbf{x}_0^w), \mathbf{x}_t^l \sim q(\mathbf{x}_t^l | \mathbf{x}_0^l)} \log \sigma \left(\beta T \cdot \right. \\ & \left. \mathbb{E}_{\mathbf{x}_{t-1}^w \sim p_{\star}^w(\mathbf{x}_{t-1}^w | \mathbf{x}_t^w, c), \mathbf{x}_{t-1}^l \sim p_{\star}^l(\mathbf{x}_{t-1}^l | \mathbf{x}_t^l, c)} \left[\log \frac{p_{\theta}(\mathbf{x}_{t-1}^w | \mathbf{x}_t^w, c)}{p_{\text{ref}}(\mathbf{x}_{t-1}^w | \mathbf{x}_t^w, c)} - \log \frac{p_{\theta}(\mathbf{x}_{t-1}^l | \mathbf{x}_t^l, c)}{p_{\text{ref}}(\mathbf{x}_{t-1}^l | \mathbf{x}_t^l, c)} \right] \right) \\ = & -\mathbb{E}_{\mathbf{c} \sim \mathcal{D}(c), t \sim \mathcal{U}(0, T), \mathbf{x}_t^w \sim q(\mathbf{x}_t^w | \mathbf{x}_0^w), \mathbf{x}_t^l \sim q(\mathbf{x}_t^l | \mathbf{x}_0^l)} \log \sigma \left(\beta T \cdot \right. \\ & \left. \mathbb{E}_{\mathbf{x}_{t-1}^w \sim p_{\star}^w(\mathbf{x}_{t-1}^w | \mathbf{x}_t^w, c), \mathbf{x}_{t-1}^l \sim p_{\star}^l(\mathbf{x}_{t-1}^l | \mathbf{x}_t^l, c)} \left[\log \frac{p_{\theta}(\mathbf{x}_{t-1}^w | \mathbf{x}_t^w, c)}{p_{\star}^w(\mathbf{x}_{t-1}^w | \mathbf{x}_t^w, c)} - \log \frac{p_{\star}^w(\mathbf{x}_{t-1}^w | \mathbf{x}_t^w, c)}{p_{\text{ref}}(\mathbf{x}_{t-1}^w | \mathbf{x}_t^w, c)} \right. \right. \\ & \left. \left. - \left(\log \frac{p_{\theta}(\mathbf{x}_{t-1}^l | \mathbf{x}_t^l, c)}{p_{\star}^l(\mathbf{x}_{t-1}^l | \mathbf{x}_t^l, c)} - \log \frac{p_{\star}^l(\mathbf{x}_{t-1}^l | \mathbf{x}_t^l, c)}{p_{\text{ref}}(\mathbf{x}_{t-1}^l | \mathbf{x}_t^l, c)} \right) \right] \right) \\ = & -\mathbb{E}_{\mathbf{c} \sim \mathcal{D}(c), t \sim \mathcal{U}(0, T), \mathbf{x}_t^w \sim q(\mathbf{x}_t^w | \mathbf{x}_0^w), \mathbf{x}_t^l \sim q(\mathbf{x}_t^l | \mathbf{x}_0^l)} \log \sigma \left(-\beta T \cdot \right. \\ & \left. \mathbb{D}_{\text{KL}}(p_{\star}^w(\mathbf{x}_{t-1}^w | \mathbf{x}_t^w, c) \| p_{\theta}(\mathbf{x}_{t-1}^w | \mathbf{x}_t^w, c)) - \mathbb{D}_{\text{KL}}(p_{\star}^w(\mathbf{x}_{t-1}^w | \mathbf{x}_t^w, c) \| p_{\text{ref}}(\mathbf{x}_{t-1}^w | \mathbf{x}_t^w, c)) \right. \\ & \left. - \left(\mathbb{D}_{\text{KL}}(p_{\star}^l(\mathbf{x}_{t-1}^l | \mathbf{x}_t^l, c) \| p_{\theta}(\mathbf{x}_{t-1}^l | \mathbf{x}_t^l, c)) - \mathbb{D}_{\text{KL}}(p_{\star}^l(\mathbf{x}_{t-1}^l | \mathbf{x}_t^l, c) \| p_{\text{ref}}(\mathbf{x}_{t-1}^l | \mathbf{x}_t^l, c)) \right) \right) \end{aligned} \quad (28)$$

Using the Gaussian parameterization of the reverse process Eq. (7), the above loss simplifies to:

$$\begin{aligned} \mathcal{L}_{\text{DDSPO}}(\theta) \leq & -\mathbb{E}_{(\mathbf{x}_0^w, \mathbf{x}_0^l) \sim \mathcal{D}, \mathbf{c} \sim \mathcal{D}(c), t \sim \mathcal{U}(0, T), \mathbf{x}_t^w \sim q(\mathbf{x}_t^w | \mathbf{x}_0^w), \mathbf{x}_t^l \sim q(\mathbf{x}_t^l | \mathbf{x}_0^l)} \log \sigma \left(-\beta \cdot \left[\right. \right. \\ & \left. \left. \|\boldsymbol{\epsilon}_{\star}^w - \boldsymbol{\epsilon}_{\theta}(\mathbf{x}_t^w, t, \mathbf{c})\|_2^2 - \|\boldsymbol{\epsilon}_{\star}^w - \boldsymbol{\epsilon}_{\text{ref}}(\mathbf{x}_t^w, t, \mathbf{c})\|_2^2 - (\|\boldsymbol{\epsilon}_{\star}^l - \boldsymbol{\epsilon}_{\theta}(\mathbf{x}_t^l, t, \mathbf{c})\|_2^2 - \|\boldsymbol{\epsilon}_{\star}^l - \boldsymbol{\epsilon}_{\text{ref}}(\mathbf{x}_t^l, t, \mathbf{c})\|_2^2) \right] \right). \end{aligned} \quad (29)$$

DSPO DSPO [68] follows the standard score decomposition used in conditional diffusion models and expresses the conditional score as

$$\nabla_{\mathbf{x}_t^w} \log p_{\theta}(\mathbf{x}_t^w | \mathbf{c}, y) = \nabla_{\mathbf{x}_t^w} \log p_{\theta}(\mathbf{x}_t^w | \mathbf{c}) + \nabla_{\mathbf{x}_t^w} \log p(y | \mathbf{x}_t^w, \mathbf{c}), \quad (30)$$

where y represents a human-preference condition. DSPO proposes to fine-tune the pretrained score model to match a preference-adjusted target score, leading to the objective

$$\min_{\theta} \omega(t) \left\| \nabla_{\mathbf{x}_t^w} \log p_{\theta}(\mathbf{x}_t^w \mid \mathbf{c}) - (\nabla_{\mathbf{x}_t^w} \log p(\mathbf{x}_t^w \mid \mathbf{c}) + \gamma \nabla_{\mathbf{x}_t^w} \log p(y \mid \mathbf{x}_t^w, \mathbf{c})) \right\|_2^2, \quad (31)$$

where $\omega(t)$ is the diffusion timetable weighting function and γ scales the preference constraint. The preference likelihood is modeled as

$$p(y \mid \mathbf{x}_t^w, \mathbf{c}) = p(\mathbf{x}_t^w \succ \mathbf{x}_t^l \mid \mathbf{x}_t^l, \mathbf{c}) = \sigma(r(\mathbf{x}_t^w, t, \mathbf{c}) - r(\mathbf{x}_t^l, t, \mathbf{c})). \quad (32)$$

By substituting this likelihood into Eq. (31) and deriving the resulting score-matching objective, the loss can be extended over all timesteps to yield:

$$\begin{aligned} \mathcal{L}_{\text{DSPO}}(\theta) = & \mathbb{E}_{(\mathbf{x}_0^w, \mathbf{x}_0^l) \sim \mathcal{D}, \mathbf{c} \sim \mathcal{D}(\mathbf{c}), t \sim \mathcal{U}(0, T), \mathbf{x}_t^w \sim q(\mathbf{x}_t^w \mid \mathbf{x}_0^w), \mathbf{x}_t^l \sim q(\mathbf{x}_t^l \mid \mathbf{x}_0^l)} A(t) \left\| (\mathbf{\epsilon}_{\theta}(\mathbf{x}_t^w, t, \mathbf{c}) - \mathbf{\epsilon}^w) \right. \\ & \left. - \beta \left(1 - \sigma(r_{\theta}(\mathbf{x}_t^w, t, \mathbf{c}) - r_{\theta}(\mathbf{x}_t^l, t, \mathbf{c})) \right) \cdot (\mathbf{\epsilon}_{\theta}(\mathbf{x}_t^w, t, \mathbf{c}) - \mathbf{\epsilon}_{\text{ref}}(\mathbf{x}_t^w, t, \mathbf{c})) \right\|_2^2. \end{aligned} \quad (33)$$

Here, $A(t)$ denotes a timestep-dependent weighting function; following DSPO, we disregard $A(t)$ and the associated parameters involving α_t and β_t at the beginning of the objective. In DSPO, to avoid training an additional probability model, $r(\mathbf{x}_t, \mathbf{c})$ is computed using the implicit reward formulation of Diffusion-DPO [52]

$$r(\mathbf{x}_t, t, \mathbf{c}) = \lambda \log \frac{p_{\theta}(\mathbf{x}_{t-1} \mid \mathbf{x}_t, \mathbf{c})}{p_{\text{ref}}(\mathbf{x}_{t-1} \mid \mathbf{x}_t, \mathbf{c})}, \quad (34)$$

DSPO approximates \mathbf{x}_t using its posterior mean under the forward process as

$$\mathbb{E}[\mathbf{x}_{t-1} \mid \mathbf{x}_t, x_0] = \sqrt{\frac{\alpha_{t-1}}{\alpha_t}} \left(\mathbf{x}_t - \frac{\beta_t}{\sqrt{1 - \bar{\alpha}_t}} \mathbf{\epsilon} \right).$$

Then, using this approximation, the estimated $p_{\theta}(\mathbf{x}_{t-1} \mid \mathbf{x}_t, \mathbf{c})$ becomes

$$\lambda \left(\sqrt{2\pi\sigma_t^2} \right)^{-d} \exp \left(-\frac{1}{2} \frac{\beta_t}{1 - \bar{\alpha}_{t-1}} \frac{\alpha_{t-1}}{\alpha_t} \|\mathbf{\epsilon} - \mathbf{\epsilon}_{\theta}(\mathbf{x}_t, t, \mathbf{c})\|_2^2 \right).$$

Therefore, the reward function $r(\cdot) = \lambda(\log p_{\theta}(\mathbf{x}_{t-1} \mid \mathbf{x}_t, \mathbf{c}) - \log p_{\text{ref}}(\mathbf{x}_{t-1} \mid \mathbf{x}_t, \mathbf{c}))$ is represented in DSPO as

$$r(\mathbf{x}_t, t, \mathbf{c}) = -\frac{\lambda}{2} \frac{\beta_t}{1 - \bar{\alpha}_{t-1}} \frac{\alpha_{t-1}}{\alpha_t} \left(\|\mathbf{\epsilon} - \mathbf{\epsilon}_{\theta}(\mathbf{x}_t, t, \mathbf{c})\|_2^2 - \|\mathbf{\epsilon} - \mathbf{\epsilon}_{\text{ref}}(\mathbf{x}_t, t, \mathbf{c})\|_2^2 \right).$$

In contrast, our formulation avoids this forward-process approximation and derives the denoising target directly from the contrastive denoising policies. Specifically, instead of using $\mathbf{\epsilon}$ obtained from the forward posterior mean approximation, we incorporate a policy-grounded target $\mathbf{\epsilon}_{\star}$ extracted from the winning and losing denoising policies $p_{\star}^w(\mathbf{x}_{t-1}^w \mid \mathbf{x}_t^w, \mathbf{c})$ and $p_{\star}^l(\mathbf{x}_{t-1}^l \mid \mathbf{x}_t^l, \mathbf{c})$, respectively. This leads to a modified approximation of the form

$$\mathbb{E}[\mathbf{x}_{t-1} \mid \mathbf{x}_t, x_0] = \sqrt{\frac{\alpha_{t-1}}{\alpha_t}} \left(\mathbf{x}_t - \frac{\beta_t}{\sqrt{1 - \bar{\alpha}_t}} \mathbf{\epsilon}_{\star} \right),$$

and accordingly, the reward expression becomes

$$r(\mathbf{x}_t, t, \mathbf{c}) = -\frac{\lambda}{2} \frac{\beta_t}{1 - \bar{\alpha}_{t-1}} \frac{\alpha_{t-1}}{\alpha_t} \left(\|\mathbf{\epsilon}_{\star} - \mathbf{\epsilon}_{\theta}(\mathbf{x}_t, t, \mathbf{c})\|_2^2 - \|\mathbf{\epsilon}_{\star} - \mathbf{\epsilon}_{\text{ref}}(\mathbf{x}_t, t, \mathbf{c})\|_2^2 \right).$$

Through this replacement, the reward is directly derived from the contrastive denoising policies rather than from a forward-process approximation, enabling policy-grounded preference supervision at each denoising step.

B. Full Results

In this section, we provide the complete results omitted from the main paper due to space constraints.

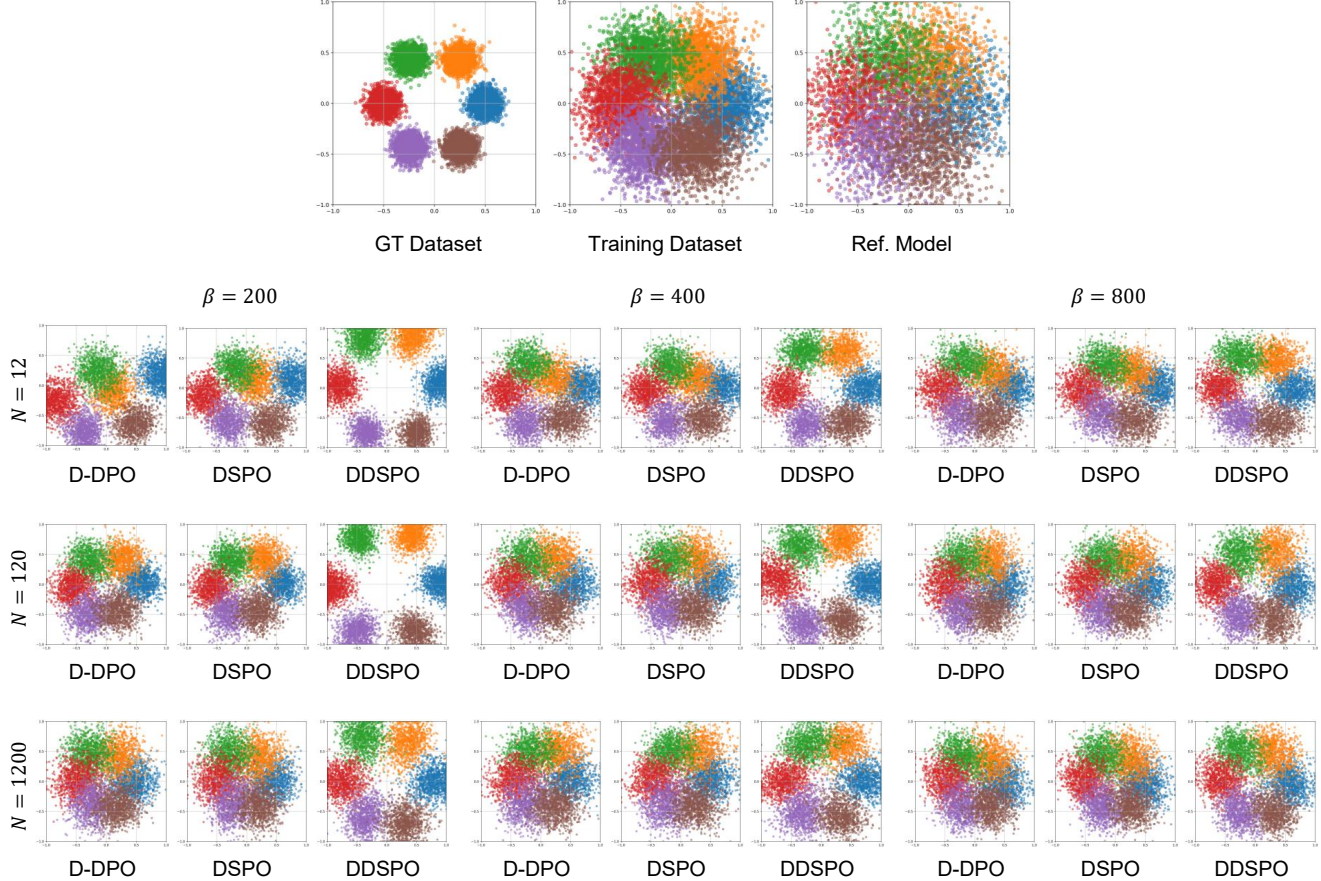


Figure A. **Full Results of Toy Experiments for Comparison of Diffusion DPO (D-DPO), DSPO and DDSPO.** Qualitative results under varying dataset size ($N \in \{12, 120, 1200\}$) and regularization strengths ($\beta \in \{200, 400, 800\}$).

Toy Experiment Results We report extended results from the 2D toy experiment introduced in Section 4.1. Specifically, we compare Diffusion DPO and DDSPO across various settings by varying the dataset size and the hyperparameter β . Fig. A presents results across different combinations of preference pair counts ($N \in \{12, 120, 1200\}$) and regularization strengths ($\beta \in \{200, 400, 800\}$).

Across all configurations, we observe that DDSPO consistently produces more well-separated and class-consistent outputs compared to Diffusion DPO. Both increasing the number of preference pairs per class (N) and the regularization strength (β) lead to improved separation for both methods, but these improvements are substantially more pronounced and stable with DDSPO. Notably, DDSPO maintains clear cluster boundaries and discriminative outputs even under low-data regimes (e.g., $N = 12$), whereas Diffusion DPO often suffers from mode overlap and distorted clusters, particularly when supervision is limited or hyperparameters are not carefully tuned. These results indicate that DDSPO is robust to the amount of supervision, consistently enabling the model to learn well-separated, condition-specific distributions by dynamically providing diverse guidance at each timestep and pushing samples away from dispreferred directions.

Text-to-Image Alignment Results As shown in Table A, our method consistently enhances the performance of all tested architectures across every subcategory of benchmarks, confirming its universal applicability and effectiveness.

In comparison to methods like IterComp and CaPO applied to the SDXL model, our method achieves superior results in the *Two Objects* and *Colors* categories of the GenEval benchmark, while slightly lagging behind in *Counting* and *Color Attribution*, which are also part of GenEval. On the T2I-Compbench benchmark, our method outperforms existing approaches in *Color*, *Shape*, and *Complex*, while showing slightly lower performance than IterComp in *Spatial* and *Non-Spatial*. Nonetheless, it achieves the highest *Overall* score.

It is worth highlighting that, unlike IterComp and CaPO—both of which rely on reward models and human-annotated

Table A. Comparison of Various Architectures and Methods on Alignment Benchmarks. We evaluate SD-1.4, SDXL and SANA models on GenEval and T2I-CompBench, each measuring alignment across six distinct aspects. The SDXL baseline is compared with variants fine-tuned using IterComp, CaPO, and our method, while the SD-1.4 and SANA baselines are compared with a version fine-tuned using our method.

(a) GenEval							
Model	GenEval						
	Single	Two	Counting	Colors	Position	Color Attribution	Overall
SD-1.4	0.98	0.35	0.32	0.73	0.05	0.07	0.4245
+DDSPo	1.00	0.53	0.44	0.81	0.12	0.13	0.5045
SDXL	0.99	0.65	0.37	0.82	0.14	0.17	0.5229
+Itercomp	1.00	0.83	0.43	0.86	0.22	0.33	0.6108
+CaPO	0.99	0.79	0.48	0.86	0.15	0.28	0.5900
+DDSPo	1.00	0.88	0.41	0.90	0.20	0.25	0.6049
SANA	0.99	0.79	0.68	0.88	0.31	0.44	0.6812
+DDSPo	1.00	0.88	0.69	0.90	0.37	0.52	0.7266

(b) T2I-Compbench								
Model	T2I-Compbench							
	Color	Shape	Texture	Spatial	Non Spatial	Complex(B-VQA)	Overall	Complex(3-in-1)
SD-1.4	0.3593	0.3589	0.4024	0.1059	0.3096	0.3792	0.3192	0.3089
+DDSPo	0.5123	0.4336	0.5425	0.1475	0.3130	0.4463	0.3992	0.3451
SDXL	0.5762	0.4774	0.5225	0.1969	0.3125	0.4253	0.4185	0.3346
+Itercomp	0.7090	0.5254	0.6249	0.2400	0.3184	0.4899	0.4846	0.3687
+CaPO	0.6460	0.5370	0.6330	0.1720	0.3120	0.4910	0.4652	-
+DDSPo	0.7658	0.5610	0.6631	0.2335	0.3175	0.4972	0.5064	0.3734
SANA	0.6987	0.5330	0.6555	0.3212	0.3146	0.5176	0.5068	0.3844
+DDSPo	0.7634	0.6001	0.7157	0.3545	0.3152	0.5563	0.5509	0.4042

Table B. Joint Improvement on Text-to-Image Alignment and Aesthetic Quality. We evaluate DDSPO trained with different types of supervision. *Rand-removal* uses 200K prompts with alignment-degraded negatives generated via random token removal. *LLaMA (AQ)* uses 200K prompts with aesthetic-degraded negatives generated via LLaMA-3. *Rand-removal + LLaMA (AQ)* combines both sources by sampling 100K examples from each dataset (alignment and aesthetic), for a total of 200K. All variants improve over the SDXL base model across both alignment and aesthetic metrics, demonstrating the flexibility of DDSPO across objectives.

Method	T2I Alignment		Aesthetic Quality	
	GenEval \uparrow	CompBench \uparrow	HPSv2 \uparrow	PickScore \uparrow
SDXL	0.5229	0.4034	27.89	22.27
Rand-removal	0.6049	0.4857	28.64	22.66
LLaMA (AQ)	0.5808	0.4698	28.78	22.70
Rand-removal + LLaMA (AQ)	0.6010	0.4863	28.79	22.69

preference data—our method requires neither. Despite this, it achieves competitive results across both GenEval and T2I-CompBench, demonstrating that strong compositional alignment can be achieved with minimal supervision through self-consistency alone.

C. Improving Both Alignment and Aesthetic Quality

To evaluate the versatility of DDSPO, we conduct a joint experiment targeting both text-to-image alignment and aesthetic quality. Specifically, we reuse the datasets introduced in Secs. 4.2 and 4.3, each containing 200K training examples constructed for alignment and aesthetic supervision, respectively. For this joint setup, we randomly sample 100K examples from each and train DDSPO on the combined 200K preference pairs. All experiments are conducted by finetuning the base SDXL [38] model.

We compare the jointly trained DDSPO model against the original SDXL model, as well as models trained using only alignment supervision (via random token removal) and only aesthetic supervision (via LLaMA-based degradation). As

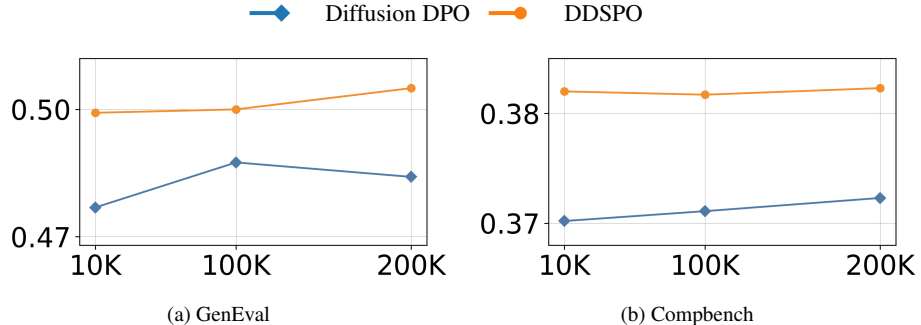


Figure B. **Ablation Study on Dataset Size** Performance on GenEval (left) and Compbench (right) with various training set sizes. The orange line denotes our method, while the blue line denotes D-DPO.

shown in Tab. B, our jointly trained DDSPO model achieves consistent improvements in both *T2I Alignment* (GenEval and CompBench) and *Aesthetic Quality* (HPSv2 and PickScore), demonstrating the effectiveness of DDSPO across diverse objectives and its ability to integrate multiple supervision signals in a unified framework.

D. Dataset Size Ablation

We performed an ablation study to evaluate the effect of training dataset size on performance, using Stable Diffusion 1.4 as the base model. As illustrated in Fig. B, we compare our method (orange) with D-DPO (blue) on the GenEval and CompBench benchmarks, using 10K, 100K, and 200K training pairs. The plotted values represent the overall alignment scores (averaged across metrics) for each benchmark.

Our method shows clear and consistent gains over D-DPO across all dataset sizes. Notably, even with only 10K preference pairs, our method achieves substantial improvements over the base model (whose GenEval and CompBench scores are 0.4245 and 0.3075, respectively), demonstrating its strong data efficiency. These results highlight the practicality and scalability of DDSPO, which remains highly effective even in low-data regimes.

E. Implementation Details

Training Configuration We fine-tune Stable Diffusion 1.4 [43], 1.5 [44], SDXL [38], and SANA [56] using $4 \times$ NVIDIA A100 GPUs for the former two and $2 \times$ NVIDIA H100 GPUs for the latter two. Full fine-tuning is applied to Stable Diffusion and SDXL models in mixed precision (fp16), while SANA is fine-tuned using LoRA [17] in full precision (fp32) with a rank of 512.

We follow the optimizer settings used in Diffusion-DPO: specifically, we use AdamW [34] for experiments with Stable Diffusion 1.5 and Adafactor [48] for SDXL. For SANA, we use AdamW as the optimizer. We use an effective batch size of 2048 pairs via gradient accumulation and train all models for 100 iterations. A linear warmup of 100 steps is applied to Stable Diffusion 1.4/1.5 and SDXL, while no warmup is used for SANA. As in Diffusion-DPO [52], the learning rate is scaled with the divergence penalty coefficient β as learning rate = $\beta/(2.048 \times 10^8)$.

As shown in Fig. C, we sweep $\beta \in [6000, 8000, 10000, 12000]$ for Diffusion-DPO and $\beta \in [14000, 16000, 18000, 20000]$ for DDSPO on Stable Diffusion 1.4. The figure shows the resulting CompBench [18] and Inception Scores (IS) [47], revealing a trade-off between alignment performance and image quality: smaller β values can improve alignment, but if β becomes too small, it often results in noticeable degradation in image quality. Outside of these ranges, we observed that image fidelity deteriorates significantly for smaller β , while alignment gains diminish for larger values. Diffusion-DPO achieves the best balance at $\beta = 8000$, while DDSPO consistently performs well at $\beta = 16000$. We adopt these values as our default configurations throughout all main experiments. The same value of $\beta = 16000$ is used to train DDSPO on SDXL, while $\beta = 2000$ is used for SANA, both of which result in stable and reliable performance.

While our default settings may not represent the global optimum, we find them to be robust across architectures and tasks. In our experiments, using a larger β combined with more training steps can match the performance of the default $\beta = 16000$, 100-step setup, but without significant gains. Optimal configurations may differ from Diffusion-DPO due to differences in both the loss formulation and the preference supervision signal—our prompt-perturbed pairs provide more explicit guidance, often requiring stronger regularization.

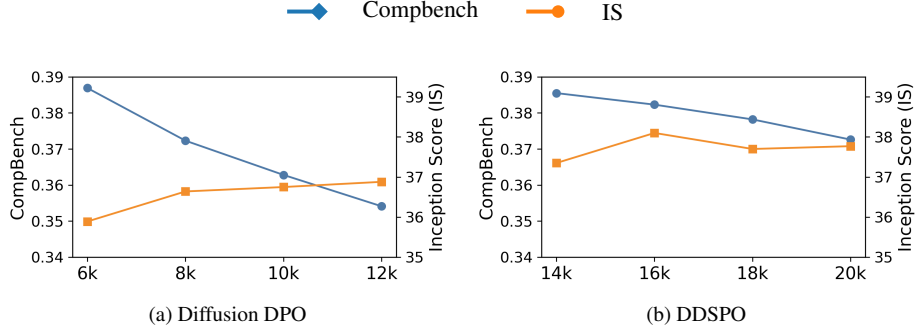


Figure C. **Ablation Study on β .** Performance on Diffusion DPO (left) and DDSPO (right) with various β . The blue line denotes Compbench score while the orange line denotes IS.

Generation and Evaluation Settings We use classifier-free guidance and DDIM sampling for all generations. For Stable Diffusion 1.4 and 1.5, we use a guidance scale of 7.5 and 25 sampling steps at a resolution of 512×512 . For SDXL, we use a guidance scale of 5.0 and 25 steps at 1024×1024 . For SANA, we use a guidance scale of 4.5 and 20 steps at 1024×1024 . These settings are used for generating both x_0^w and x_0^l during training and evaluation.

Each model is paired with its respective default scheduler: PNDMScheduler [32] for Stable Diffusion 1.4 and 1.5, EulerDiscreteScheduler [20] for SDXL, and DPMSolverMultistepScheduler [35, 36] for SANA.

We report evaluation results using publicly released weights for all baselines, including Diffusion-DPO (trained on Pick-a-Pic), DPO-KTO, and Iterative Comparison. For CaPO, which does not release model weights, we report Geneval and CompBench results as stated in the original paper.

T2I-CompBench [18] evaluates different compositional aspects using specialized metrics: BLIP-VQA [27] is used for *Color*, *Shape*, and *Texture*; UniDet [67] for *Spatial*; and CLIP [40] for *Non-Spatial*. The default protocol for measuring *Complex* is a 3-in-1 composite that combines BLIP-VQA, UniDet, and CLIP. However, CaPO [26] reports *Complex* using only BLIP-VQA. To enable fair comparison with CaPO, we follow its evaluation setting in Tabs. A and 3, using BLIP-VQA alone to compute *Complex*. For all other results, we adopt the original 3-in-1 composite as defined in CompBench, and use it to compute both the *Complex* score and the overall average. For completeness, Tab. A also includes the 3-in-1 version of *Complex*.

F. Limitation

As with Diffusion-DPO, DDSPO requires careful selection of the balancing coefficient β , which controls the trade-off between reward maximization and divergence minimization. This reliance on hyperparameter tuning can add practical complexity, often necessitating task-specific calibration.

DDSPO requires access to score-level preferences during training, which are derived from denoising scores of preferred and dispreferred policies. In this work, we construct such preferences by perturbing prompts and assuming that degraded prompts yield less desirable outputs. While this strategy enables automated supervision, it is applicable only when preferences can be effectively modeled through prompt manipulation. In tasks where such modeling is infeasible—*e.g.*, when only preferences over final outputs x_0 are available—DDSPO cannot be directly applied. Extending DDSPO to such settings may require alternative methods for obtaining score preferences, such as auxiliary reward models, preference classifiers, or contrastive distillation techniques. Exploring these directions remains a promising avenue for future research.

Compared to Diffusion DPO, which requires four score computations per preference pair—namely, $\epsilon_\theta(x_t^w, t, c)$, $\epsilon_{\text{ref}}(x_t^w, t, c)$, $\epsilon_\theta(x_t^l, t, c)$, and $\epsilon_{\text{ref}}(x_t^l, t, c)$ —DDSPO introduces one additional computation: $\epsilon_{\text{ref}}(x_t^l, t, c^-)$. This results in approximately 25% more computation per training step. In practice, DDSPO achieves strong performance with just 200K pseudo-preference pairs and 100 training steps—significantly less data and computation than prior work, which often uses 800K pairs and over 1,000 steps. On SDXL, generating the 200K pairs took approximately 5 H100-days, and training for 100 steps required an additional 1 H100-day.



Figure D. **Prompt Perturbation Examples and Corresponding Generations.** Each column shows an original prompt c and its perturbed version c^- produced using different strategies—Random Removal, LLaMA-Align, and LLaMA-Aesthetic. Images are generated using SDXL for each prompt pair.

G. Prompt Perturbation

To construct supervision signals for DDSPO, we perturb prompts to produce semantically or aesthetically degraded variants. For each original prompt c , we generate a corresponding negative prompt c^- that is intended to yield lower-quality or misaligned images. We adopt two perturbation strategies depending on the supervision objective.

Alignment Degradation (Random Removal) For alignment supervision, we generate negative prompts by randomly removing 40–70% of the tokens from the original prompt. This lightweight corruption introduces ambiguity and reduces semantic specificity, resulting in weaker text-to-image alignment.

Alignment Degradation via LLM We also leverage LLaMA3-8B [10] to generate semantically degraded prompts that obscure key visual concepts. As shown in Fig. Ea, the instruction guides the model to remove or generalize important elements, while preserving the overall structure of the original prompt. This allows us to obtain more compositional and realistic misalignment cases compared to random token deletion.

Aesthetic Degradation via LLM To supervise visual quality, we again use LLaMA3-8B to rewrite prompts in a way that intentionally reduces aesthetic appeal. The instruction template, shown in Fig. Eb, directs the model to degrade aspects like color, lighting, texture, and clarity while preserving the subject. This produces visually inferior prompts in a controlled and targeted way.

These perturbation techniques allow us to generate rich and scalable preference data without requiring manual annotations. Example prompt pairs are provided in Fig. D.

H. Qualitative Results

We present qualitative comparisons of generated images from SD-1.4, SDXL, and SANA across both alignment and aesthetic settings. To ensure fair comparison, all images in each set are generated using the same random seed. For alignment, Fig. F shows results from SD-1.4 alongside diffusion DPO and DDSPO trained using prompt perturbation, while Figs. G and H compare DDSPO with each corresponding base model (SDXL and SANA). For aesthetic comparisons, Fig. I presents results from DDSPO and its base model SDXL. Fig. J shows results from Diffusion DPO trained with Pick-a-Pic and DDSPO, which does not use Pick-a-Pic, demonstrating that DDSPO can achieve strong aesthetic improvements even without human-annotated data. All images are generated using prompts from Pick-a-Pic, except for Fig. H, which uses prompts from both the Pick-a-Pic and GenEval benchmarks.

```

1  <|begin_of_text|>
2  <|start_header_id|>system<|end_header_id|>
3  You are a helpful assistant trained to rewrite image generation prompts into *compositional negative prompts*.
4
5  Your task is to generate a list of **negative prompts** that intentionally remove or generalize important
   elements from the original prompt.
6
7  Instructions:
8  1. Identify the **important words** (nouns or adjectives) central to the image composition.
9  2. Generate negative prompts that remove or alter these important words.
10 3. Keep the structure and style of the original prompt where possible.
11 4. If the prompt is too vague (e.g., "a macaw"), return an empty list.
12
13 Format your response as:
14 Important words: [...]
15 Final output:
16 {"neg_prompts": [...]}
17
18 No extra explanations or notes.
19 ]
20
21 Below is the new prompt to process.
22 prompt: <input prompt>
23 <|eot_id|>
24 <|start_header_id|>assistant<|end_header_id|>

```

(a) Instruction template for compositional degradation using LLaMA3-8B.

```

1  <|begin_of_text|>
2  <|start_header_id|>system<|end_header_id|>
3  You are a helpful assistant trained to rewrite image generation prompts into two sets of outputs:
4
5  1. A list of **positive prompts** that enhance the aesthetic quality.
6  2. A list of **negative prompts** that degrade the aesthetic quality.
7
8  Instructions:
9  - Focus on aesthetic aspects like clarity, lighting, texture, resolution.
10 - Do NOT change the subject or meaning.
11 - For positive prompts, enhance descriptors.
12 - For negative prompts, reduce quality with terms like "blurry", "washed out", etc.
13
14 Format your response as:
15 Final output:
16 {
17   "positive_prompts": [...],
18   "neg_prompts": [...]
19 }
20
21 No extra explanations or notes.
22
23 Below is the new prompt to process.
24 prompt: <input prompt>
25 <|eot_id|>
26 <|start_header_id|>assistant<|end_header_id|>

```

(b) Instruction template for aesthetic degradation using LLaMA3-8B.

Figure E. **Instruction Templates for Semantically Degrading Prompts.** Top: alignment-focused prompt perturbation using compositional degradation. Bottom: aesthetic-focused prompt perturbation targeting quality attributes. Both are used to construct pseudo-preference pairs for DDSPO training via LLaMA3-8B.

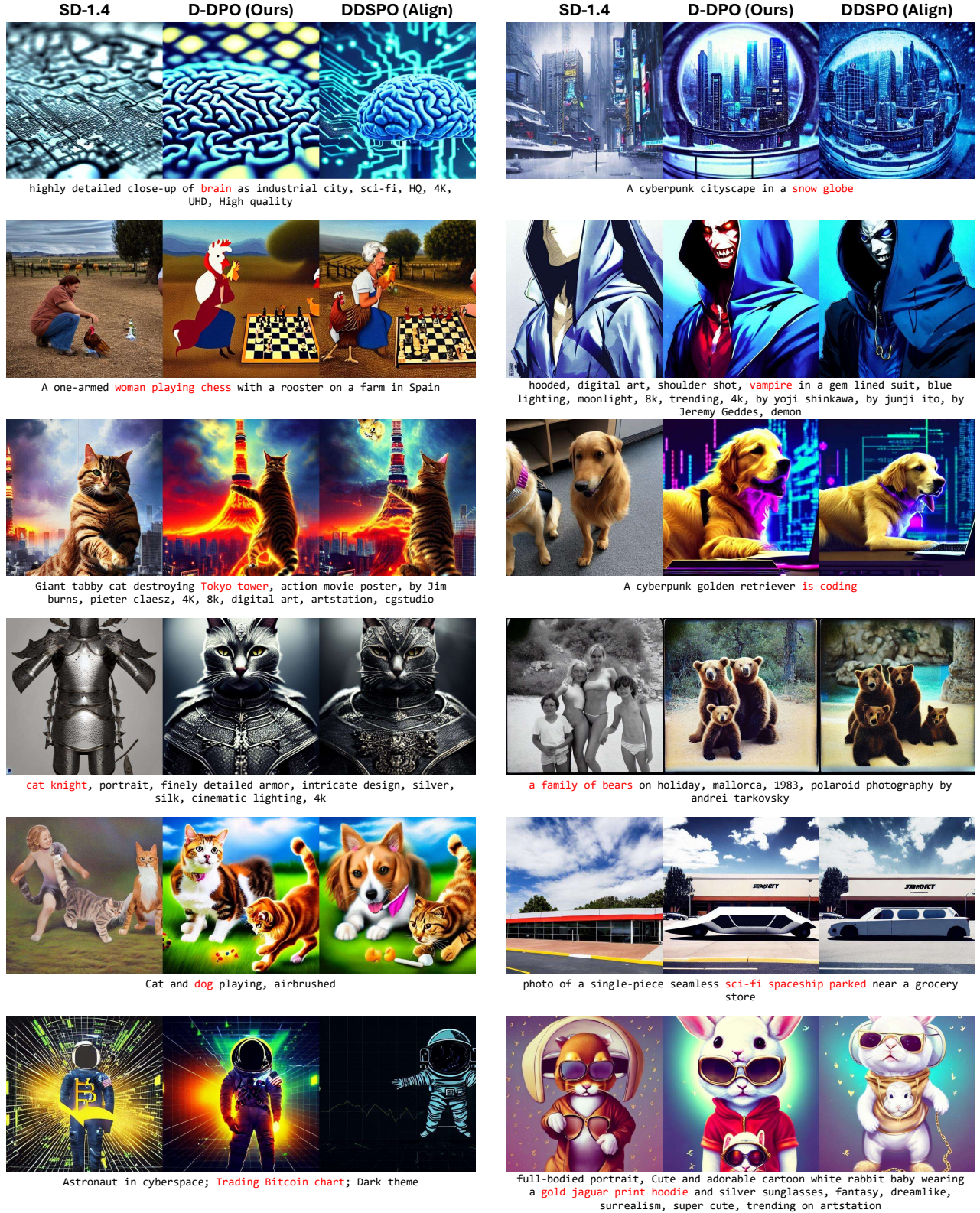


Figure F. **Qualitative Alignment Comparison between SD-1.4, D-DPO, and DDSPO.** Qualitative comparison of alignment results for SD-1.4 (left in each pair), D-DPO (middle), and DDSPO (right). Both D-DPO and DDSPO are trained using prompt perturbation. Text highlighted in red indicates key objects or attributes that were missing from the SD-1.4 outputs.

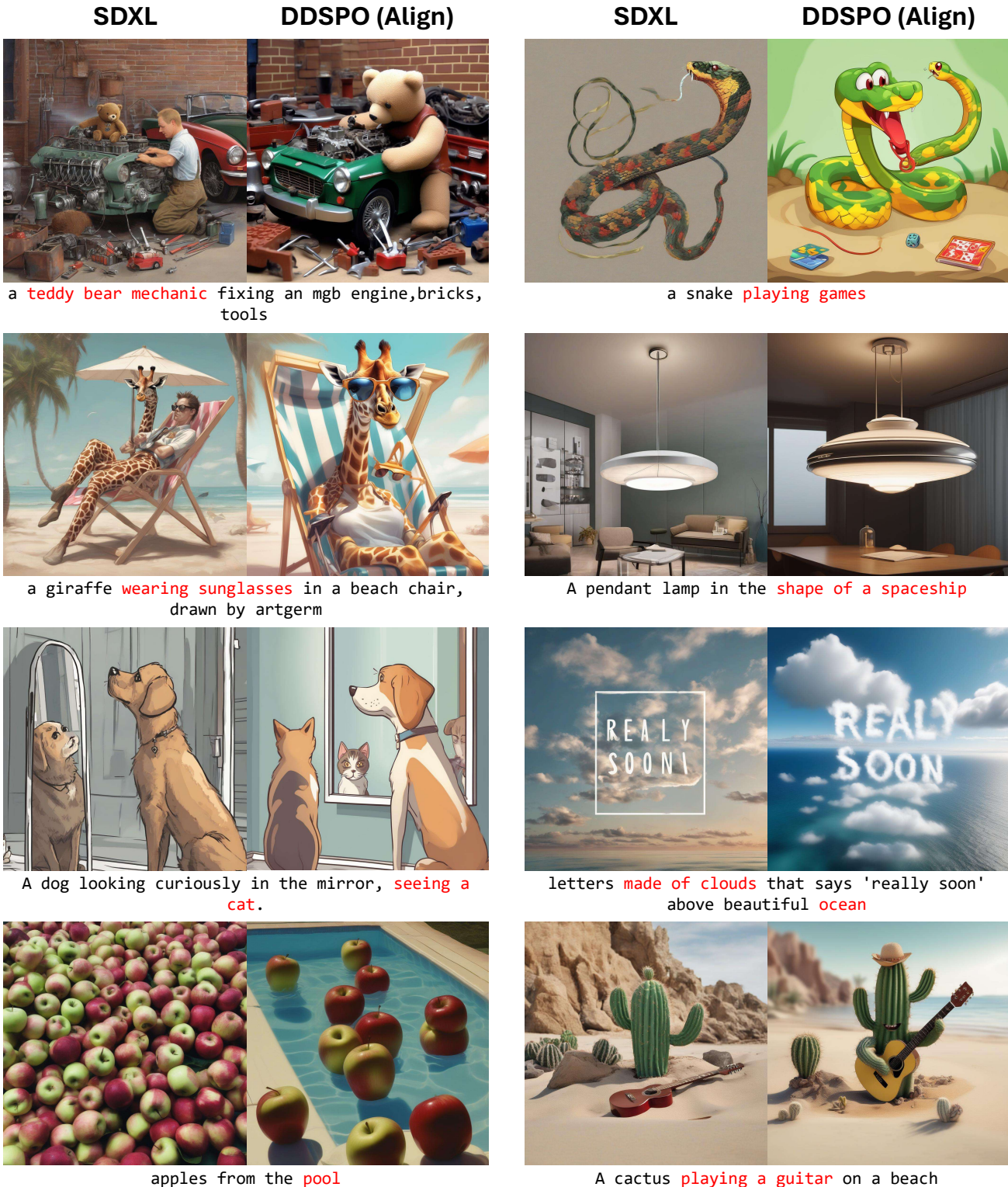


Figure G. **Qualitative Alignment Comparison between SDXL and DDSPO.** Qualitative comparison of alignment results for SDXL (left in each pair) and DDSPO (right in each pair). Text highlighted in red indicates key objects or attributes that were missing from the SDXL outputs.

SANA

a photo of an **orange** cow and a **purple** sandwich

DDSPO (Align)**SANA**

a photo of a **baseball bat** and a **fork**

DDSPO (Align)

40 year old men high tech play soccer logo



A bird with **8** spider legs



a cowboy holding a sign that "**Hunt**"



bitcoin surfing huge wave with a sea turtle

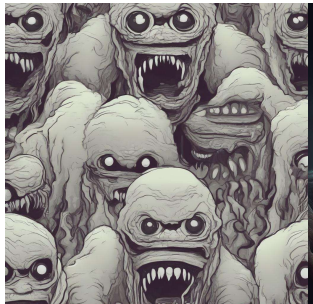


a photo of a **toothbrush** and a **bench**



a photo of a **green** teddy bear and a **brown** kite

Figure H. **Qualitative Alignment Comparison between SANA and DDSPO.** Qualitative comparison of alignment results for SANA (left in each pair) and DDSPO (right in each pair). Text highlighted in red indicates key objects or attributes that were missing from the SANA outputs.

SDXL**DDSPO (Aesthetic)**

scary monster

SDXL**DDSPO (Aesthetic)**

best quality, masterpiece, realistic, 1 girl, brown hair, brown eyes, Front, detailed face, beautiful eyes



film still from romantic 90s sitcom



An underwater city with fish swimming around



Giant ice cream cone melting and creating a river through a city



A sunset that is shattered like a broken mirror



a photograph of teddy bear riding a mini car toy in the jungle river, smiling teddy



owl in manhattan, diving through streets, close-up, motion blur, amazing nature photo

Figure I. Qualitative Aesthetic Comparison between SDXL and DDSPO. Qualitative comparison of aesthetic results for SDXL (left in each pair) and DDSPO (right in each pair) on selected prompts.

D-DPO (Pickapic) DDSPO (Aesthetic)



an arctic fox carrying a lantern using its mouth

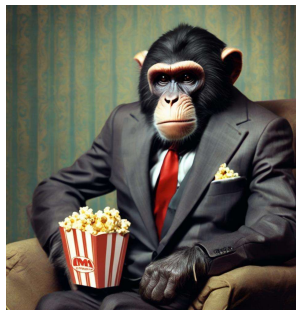
D-DPO (Pickapic) DDSPO (Aesthetic)



a fairy



A steampunk octopus playing the drums on a beach



gentleman ape monkey in a suit and tie; monkey eating AMC popcorn while watching a movie



Fantasy castle on a hilltop



A seemingly weak red-haired knight to save his girlfriend princess



radiant glowing little girl filled with swirling coronal light



Father and daughter watching the moon rise over the ocean

Figure J. Qualitative Aesthetic Comparison between D-DPO and DDSPO. Qualitative comparison of aesthetic results for D-DPO (left in each pair) and DDSPO (right in each pair). D-DPO is trained using human-annotated data from Pick-a-Pic, whereas DDSPO achieves competitive results without relying on any human annotations.